HYPOPLASTIC LEFT HEART SYNDROME: COMPONENT MODELS FOR CARDIOVASCULAR SYSTEMS AFTER THE NORWOOD PROCEDURE

by

Shawn W. Abernethy Jr.

A thesis submitted to the Faculty of the University of Delaware in partial fulfillment of the requirements for the degree of Master of Science in Applied Mathematics

Summer 2013

HYPOPLASTIC LEFT HEART SYNDROME: COMPONENT MODELS FOR CARDIOVASCULAR SYSTEMS AFTER THE NORWOOD PROCEDURE

by

Shawn W. Abernethy Jr.

Approved: ______________________________

Tobin A. Driscoll, Ph.D.
Professor in charge of thesis on behalf of the Advisory Committee

Approved: ______________________________

John A. Pelesko, Ph.D.
Chair of the Department of Mathematical Sciences

Approved: ______________________________

George H. Watson, Ph.D.
Dean of the College of Arts and Sciences

Approved: ______________________________

James G. Richards, Ph.D.
Vice Provost for Graduate and Professional Education

ACKNOWLEDGMENTS

First and foremost, I would like to thank my wife, Sarah Abernethy for her love and support during the past four years. I look forward to our new adventures in life and our future sleepless nights due to our soon to-be little one, rather than mathematics.

I would like to thank Dr. Tobin Driscoll for his patience and guidance over the past year of work on this thesis. Thank you for bringing me onto this joint project between the university and Nemours. I am thankful for Dr. Michael McCulloch for sharing his knowledge, working with us, and making time in his more than busy schedule. I am also grateful for the help and support Dr. Gilberto Schleiniger has provided throughout this project as well as the early support from Dr. William Santamore. I would not have been able to do this without my manager at The SI Organization, Inc., Marcella Maguire. Thank you for your support and affording me the flexibility in my work schedule to take all those classes the past four years. Thank you to my company, The SI Organization, Inc. for funding my graduate education. Thank you to my good friend, Bryan Petrak for providing his advice and support during these four years.

Finally, there have been many influences on my mathematical journey here at the University of Delaware, Elizabethtown College, and other places. While not listed here, I am grateful for all of their help, support, and teaching along the way.

TABLE OF CONTENTS

LIST OF TABLES

LIST OF FIGURES

ABSTRACT

The goal of the Norwood procedure is to provide systemic circulation in a cardiovascular system with a single ventricle. This procedure is universally performed on the patient population of newborns with a underdeveloped left ventricle, Hypoplastic Left Heart Syndrome (HLHS). Two alternative surgical methods are employed to provide the pulmonary circulation, Right Ventricle-Pulmonary Artery Conduit method and the Blalock-Taussig Shunt method. The objective of this study is to take a previous compartment model of the two cardiovascular systems, verify the physiology and accuracy of the system of ordinary differential equations, implement a simulator based on the mathematical model, and evaluate the model's capacity to produce a realistic right ventricular pressure-volume loop. A MATLAB based software tool was written to model both procedures and provide a graphical user interface for others in clinical practice. An optimizer was used to adjust the parameters in order to produce a pressure-volume loop comparable to expectations. Once a reasonable P-V loop was obtained for each model, the physiological realism of the model was analyzed to discover its validity and limitations.

Chapter 1

INTRODUCTION

Hypoplastic left heart syndrome (HLHS), a congenital heart defect characterized by underdevelopment of the left ventricle and associated components, is the most common lethal cardiac malformation in the newborn period [TMR+01]. Palliative surgical intervention begins within the first week of life to prevent the circulatory collapse that universally occurs if these patients are untreated [APH05] [BKD+09]. However, despite decades of experience, the one year mortality rate is still unacceptably high at 30%, due in part to inadequate assessment measurements available to the clinician.

1.1 Normal Cardiovascular System

In typical newborn cardiovascular circulation, there are two pumps (ventricles) in series. The right ventricle receives partially deoxygenated blood from the right atrium and pumps it to the pulmonary arteries and lung capillaries, which comprises the lung or *pulmonary* circulation. The now oxygenated blood moves through the pulmonary veins into the left atrium. The left ventricle then receives this oxygenated blood and pumps it to the body or *systemic* circulation. From the systemic arteries, oxygenated blood traverses capillaries of the various systemic organs (i.e. brain, kidneys, etc.) and enters the systemic veins partially deoxygenated. The deoxygenated blood in the systemic veins then enters the right atrium [LB92]. Typical heart function is illustrated in Figure 1.1.

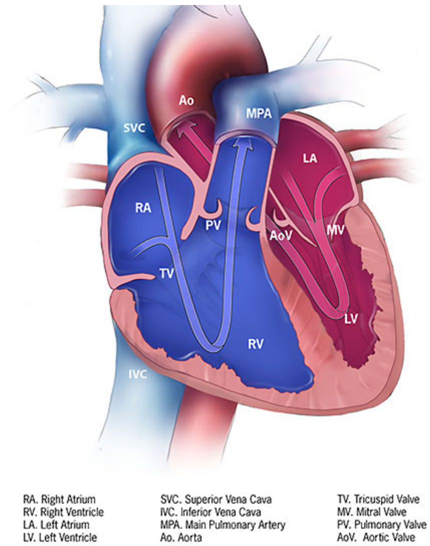

Figure 1.1: Illustration of the four chambers of a healthy heart, valves, and connecting blood vessels. The direction of bloodflow from the veins through the atria and into the arteries for both left and right side of the heart is shown with the arrow [Dis11].

1.2 HLHS Cardiovascular System

As is true in normal cardiac development, newborns with HLHS have a connection between the left and right atria known as the foramen ovale. This opening is illustrated as the red arrow between the left atrium and the right atrium in Figure 1.2. The pulmonary artery and aorta are also connected by a large blood vessel, the ductus arteriosus (PDA in Figure 1.2). Oxygenated blood enters the left atrium from the lungs and mixes with deoxygenated blood in the right atrium via the foramen ovale. When the mixed blood is ejected by the right ventricle through the pulmonary artery to be circulated through the lungs, a portion of the blood enters the aorta through the PDA and enters the systemic circulation [OSM+10].

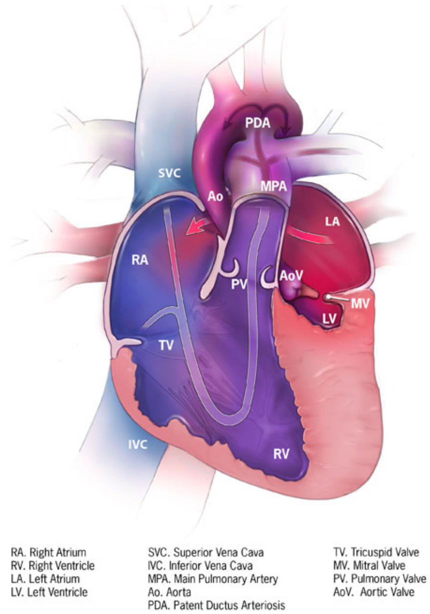

Figure 1.2: Illustration of the single ventricle heart of a newborn with HLHS. The flow of blood from the left atrium (LA) into the right atrium (RA) via the foramen ovale is shown with an arrow. The flow of blood from the systemic veins through the right atrium (RA), into the right ventricle (RV) and into the main pulmonary artery (MPA) is shown with a line [Dis11].

These naturally occurring connections between the left and right side of the heart allow for early survival of patients with HLHS [BKD+09]. Without intervention, these two communications become progressively restricted, producing inadequate delivery of oxygenated blood flow to the systemic circulation [EMS+07]. A series of three staged palliative surgical interventions is used to provide pulmonary and systemic blood flow within the challenging confines of a single ventricle circulation. Specifically, the single ventricle is burdened with both systemic and pulmonary circulations in parallel as opposed to series (healthy heart) [APH05]. This thesis focuses on the physiology created by the first of these interventions.

The first stage or *Norwood procedure* is universally performed in this patient population and is designed to produce an unobstructed connection between the single right ventricle and systemic circulation, and between the systemic and pulmonary venous circulations [BKD+09]. The surgical options for providing pulmonary blood flow, however, are complex and controversial [MMW+11] [EMS+07] [BKD+09]. The two surgical options of the Norwood procedure performed on this patient population include either a systemic to pulmonary arterial shunt (Blalock-Taussig or BT shunt) or a conduit between the right ventricle and pulmonary artery (RV-PA conduit) [EMS+07]. Both options are associated with short and long-term complications that prevent either from being considered decisively superior [OSM+10].

There have been previous attempts at modeling the normal cardiovascular system, [SLH11] [FLTV06] [SSB07] as well as a patient with a HLHS cardiovascular system, [BMdL+08] [HCC+11]. The modeling approach discussed in this thesis is the resultant circulatory system after the Norwood procedure. It closely mirrors the one presented in [Kad12]. The model presented in [Kad12] is in the form of a system of ordinary differential equations, representing a lumped or *zero-dimensional* (0D) model that was implemented in Simulink converted to MATLAB. We found the system as presented failed to conserve total volume due to an error in the connection of the coronary blood vessel. Judging the inclusion of the coronary in the model to have a minor effect on the overall dynamics, we removed it from our model and were then able to observe periodic dynamics.

The eventual goal of the work described in this thesis is to produce a computational model of the HLHS heart and circulation that could be customized in real time to an individual patient at bedside. Currently, the diagnostic tools available to physicians are unable to give adequate advance warning of serious and potentially fatal complications.

Our main criterion for evaluating the model is the generation of a right ventricle pressure-volume loop (P-V loop) that closely resembles that expected for patients with HLHS. These loops are theoretical analysis tools in which the work done by the ventricle is represented by the enclosed area of the loop [Khu06].

1.3 The Ventricular Pressure-Volume Loop

The P-V loop is a 2-dimensional representation of ventricle dynamics in the variables of pressure and volume. Physiologically, the P-V loop represents the ventricular response to changes in systemic afterload (pressure) and ventricular filling (volume) [Iai09]. This is an alternative to showing ventricular volume and pressure as functions of time.

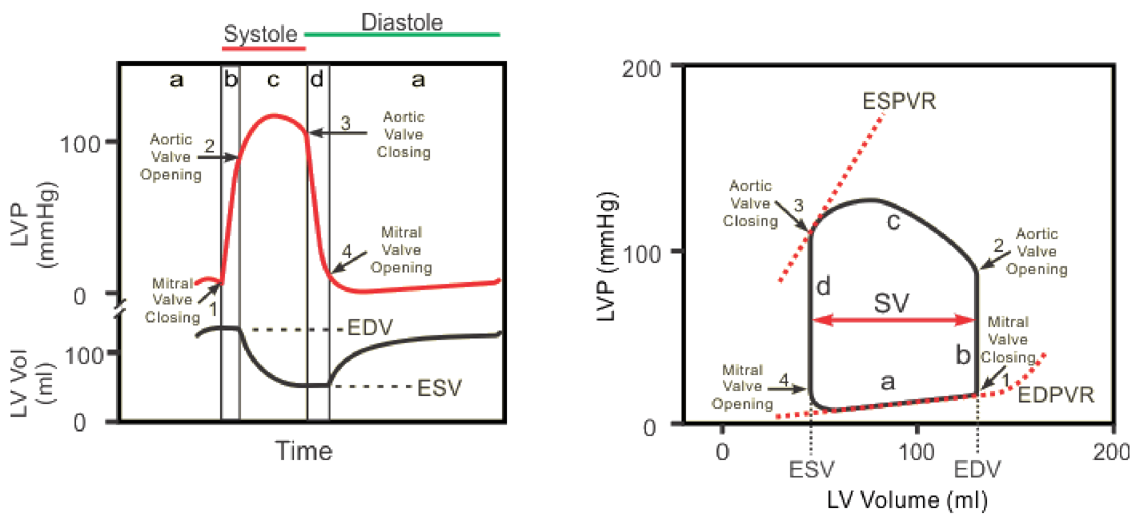

Figure 1.3: An example of a volume and pressure as functions of time are shown on the left and the the corresponding ventricular P-V loop on the right. In the time based diagram, the ventricular pressure is in red and the ventricular volume in black. In the P-V loop, the stroke volume of the ventricle is shown with the double-sided arrow. In both figures, corresponding sections of the P-V loop and time based diagram are labeled with letters *a*-*d* and corresponding events numbered 1-4 [Kla11].

The diagram of volume and pressure as functions of time show the two main phases of the ventricle: *Systole* (markers 1 to 3 on the P-V loop) and *Diastole* (3 to 1 on the P-V loop). Systole is the period in which the ventricle is full, builds pressure through ventricular contraction and ejects the blood (marked *b* and *c* in both diagrams in Figure 1.3). Diastole is the period when the ventricle is relaxing and releasing pressure while filling with blood (*d* and *a* in both diagrams in Figure 1.3) [LB92].

Section b is known as *isovolumic contraction time* (IVCT), during which there is a rapid increase in pressure created by ventricular contraction without change in ventricular volume. The onset of IVCT coincides with the closing of the mitral valve in the left ventricle (tricuspid valve in the right ventricle), and continues until the opening of the aortic valve in the left ventricle (pulmonary valve in the right ventricle). Since there is no change in volume (in a healthy heart), this part of the P-V loop is a vertical line [LB92].

Section c on both diagrams of Figure 1.3 is composed of two phases of ejection of blood from the ventricle, *rapid ejection*, the initial large reduction in volume, and *reduced ejection*, which coincides with a slight reduction in ventricular pressure. Ejection is the result of the aortic valve opening (pulmonary valve in the right ventricle), and finishes once the valve is closed. The volume of blood dispersed from the ventricle during this time is known as the *stroke volume* (SV) [LB92]. Furthermore, the total volume of blood pumped out of the ventricle per minute, *cardiac output* (CO), is computed as the product of the heart rate (HR) in beats per minute and the stroke volume [AMSA13]:

$$CO = HR \times SV.$$

Section d (between 3 and 4 on both diagrams of Figure 1.3) is known as the *isovolumic relaxation time* (IVRT). Both the aortic valve (pulmonary valve) and mitral valve (tricuspid valve) are closed, so there is no change in ventricular volume. However, since the ventricle is relaxing, there is a rapid decrease in the ventricular pressure. Once the mitral valve (tricuspid valve) opens, the ventricle begins to fill (section a on the diagrams of Figure 1.3) [LB92].

In Chapter 2, we will introduce the models for the RV-PA conduit and BT shunt as well as their derivations. Chapter 3 we describe the implementation of these models in MATLAB. Chapter 4 we then show the results of the models. And finally, Chapter 5 we suggest methods to improve the models and list future tasks.

Chapter 2

MATHEMATICAL MODELS

2.1 Hemodynamics

Assuming blood is an incompressible Newtonian fluid, the steady flow Q of blood, through a cylindrical compliant vessel can be expressed according to Poiseuilles law:

$$Q = \frac{\pi r^4 \left(P_{in} - P_{out}\right)}{8\eta l}, \tag{2.1}$$

where r and l are the radius and length of the cylindrical vessel, respectively, η is the blood viscosity and $P_{in} - P_{out}$ is the pressure difference [Mil90]. An analogy to a hydraulic system can be drawn by defining the hydraulic resistance as

$$R = \frac{8\eta l}{\pi r^4}, \tag{2.2}$$

thus defining the flow of blood through cylindrical tube as [Mil90]

$$Q = \frac{P_{in} - P_{out}}{R} = \frac{\Delta P}{R}. \tag{2.3}$$

More fundamentally, the equations for pressure and flow through a cylindrical compliant vessel can be derived from the Navier-Stokes equation for incompressible fluid. We summarize here the development given by Formaggia and Venezianni [FV03]. The Navier-Stokes equations in three dimensions are

$$\rho\left(\frac{\partial v}{\partial t} + v \cdot \nabla v\right) = -\nabla p + \mu \nabla^2 v + f \tag{2.4}$$

$$\nabla \cdot v = 0. \tag{2.5}$$

Consider Figure 2.1. The sections Γ_{in} and Γ_{out} are the openings of the vessel that connect to the previous and next vessel, respectively. The section Γ_w is the compliant wall of the blood vessel and the axis z denotes the radial direction. Blood flow through this vessel, where the blood is assumed to be an incompressible fluid can be described by equations (2.4)-(2.5).

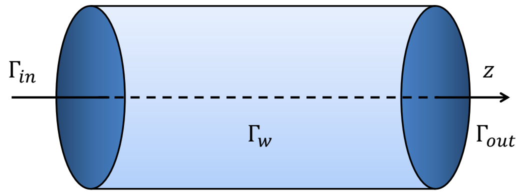

Figure 2.1: Cylindrical compliant vessel [FV03]

We make the following assumptions:

- The vessel has symmetry about the z-axis.
- The fluid moves only in the z direction.
- The z-axis is fixed with time.
- The pressure of the vessel P is dependent only on z and time, t.
- The external forces attributed to the body can be ignored.
- The velocity component orthogonal to the z-axis is negligible and dominated by the velocity in the z-direction.

From these one can derive the following one-dimensional partial differential equations:

$$\frac{\partial A}{\partial t} + \frac{\partial Q}{\partial z} = 0 \tag{2.6}$$

$$\frac{\partial Q}{\partial t} + \alpha \frac{\partial}{\partial z}\left(\frac{Q^2}{A}\right) + \frac{A}{\rho}\frac{\partial P}{\partial z} + K_R \frac{Q}{A} = 0 \tag{2.7}$$

where the unknowns A, P and Q represent the area of the cross-section of the blood vessel, pressure and flow of blood at that cross-section at time t, respectively. ρ is the blood density, K_R the friction experienced from of the vessel's wall's, and α momentum-flux correction coefficient [FV03].

Still, equations (2.6) and (2.7) are nonlinear and impossible to solve in closed form. To derive a more tractable model, we make the following additional assumptions:

- The displacement of the wall is algebraically related to the pressure.
- The convective terms' contribution are negligible.
- The variations of P and Q are much larger than the variations of A and z.

Applying these assumptions and linearizing around the trivial steady solution leads to

$$C\frac{dP}{dt} + Q_{out} = Q_{in} \tag{2.8}$$

$$L\frac{dQ}{dt} + RQ + P_{in} = P_{out}. \tag{2.9}$$

These equations are directly analogous to a linear model of an RLC circuit. The resistance R expresses dissipative loss due to blood viscosity. The compliance C represents the storage of blood due to elastic expansion of the vessel walls. The inertance L expresses the relative significance of inertia within the vessel. If we ignore inertial effects by setting $L = 0$ and solving for Q in equation (2.9), we again derive equation (2.3):

$$Q = \frac{P_{in} - P_{out}}{R} = \frac{\Delta P}{R}. \tag{2.10}$$

Also, solving for $\frac{dP}{dt}$ in equation (2.8),

$$\frac{dP}{dt} = \frac{Q_{in} - Q_{out}}{C} = \frac{1}{C}\frac{dV}{dt} = E\frac{dV}{dt}, \tag{2.11}$$

$$P = EV. \tag{2.12}$$

where E is the vessel's elastance (inverse of the compliance).

2.2 Cardiovascular System

Our model of the circulatory system consists of twelve compartments. Three of the twelve compartments represent the left atrium, right atrium, and right ventricle. The rest of the circulatory system consists of the aorta, shunt or conduit, pulmonary arteries, pulmonary capillaries, pulmonary veins, upper and lower systemic capillaries, and the superior and inferior vena cava.

2.2.1 Modeling the Blood Vessels

The pressure and flow at the entrance of the vessel Γ_{in} in Figure 2.1 are computed as shown in equations (2.10) and (2.11). The pressure and flow at the exit of one blood vessel are assumed to be the pressure and flow at the inlet of the next blood vessel. Finally, the rate of volume change of the blood at the center of the compartment is computed as the difference between the flow at the entrance and the flow at the exit of the blood vessel,

$$\dot{V}(t) = Q_{in}(t) - Q_{out}(t). \tag{2.13}$$

2.2.2 Modeling the Heart Chambers

The heart chambers experience two phases: *contraction* and *relaxation*. Contractility is the gold standard measure of ventricular function and was modeled by Suga and Sagawa [SS74] using time varying elastance. The equations to compute elastance for each of the heart chambers are defined via:

$$E_{i,h}(t) = E_{max,i,h} \max\{0, -3.374 t_{n,i,h}(t)^3 + 6.568 t_{n,i,h}(t)^2 - 1.934 t_{n,i,h}(t)\}, \tag{2.14}$$

where $i = 1, 2, 3$ represents the selection of the heart chamber, $E_{max,i,h}$ is the contractility index of the chamber, time $t \in [0, RR]$, $t_{n,i,h}(t)$ the normalized time and RR is the duration of one heartbeat [SSB07] (i.e. 1000 microsecond (μs) duration is equivalent to 60 beats per minute (bpm)).

The normalized time variables from equation (2.14) are specified in each heart chamber as [San12]:

$$t_{n,1,h}(t) = f \cdot \frac{t - (0 - 0.03)}{STI}, \; f = 3, \; STI = 0.27 \tag{2.15}$$

$$t_{n,2,h}(t) = f \cdot \frac{t - (0.02 - 0.03)}{STI}, \; f = 3 \; STI = 0.27 \tag{2.16}$$

$$t_{n,3,h}(t) = \frac{t - (0.08 - 0.0531)}{STI}, \; STI = 0.27. \tag{2.17}$$

The parameter STI is the *systolic time interval*. This is a readily measured estimate of cardiac function, with lower values implying better contractility [ALSE72]. Substituting each of the equations (2.15)-(2.17) into equation (2.14) for $t \in [0, RR]$, where RR is the period of one heartbeat in microseconds, produces Figure 2.2.

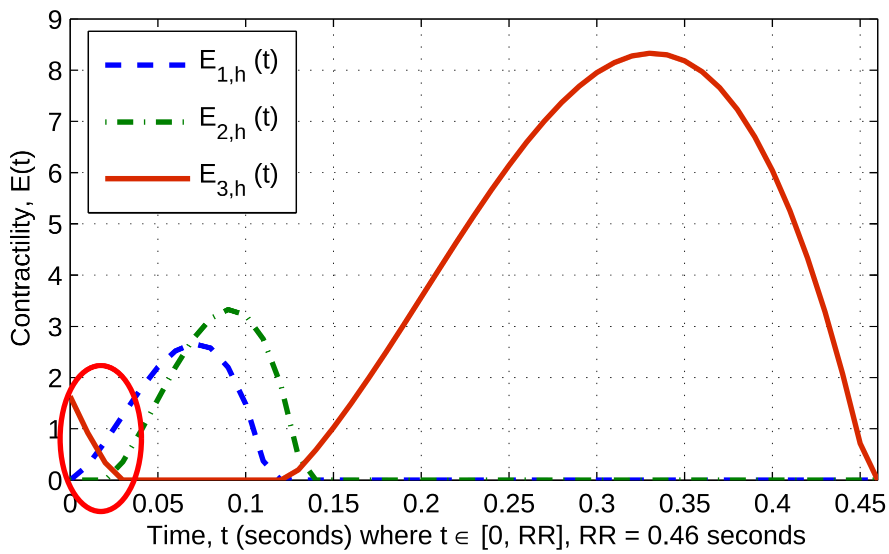

Figure 2.2: Time varying elastance of the heart chambers. The elastance vs. time for the left atrium is shown blue, right atrium green, and right ventricle in red.

Circled in Figure 2.2 is a positive artifact that should be zero to represent the contractility of the right ventricle during diastole. To give $E_{3,h}$ the desired periodic behavior ($E_{3,h}(0) = E_{3,h}(RR)$), an indicator function was used to modify the new equation for $E_{3,h}$:

$$E_{3,h}(t) = I(t) E_{max,i,h} \max\{0, -3.374 t_{n,i,h}(t)^3 + 6.568 t_{n,i,h}(t)^2 - 1.934 t_{n,i,h}(t)\}, \tag{2.18}$$

$$\text{where } I(t) = \begin{cases} 0 & t \in [0, 0.05]\,, \\ 1 & t \in (0.05, RR]\,. \end{cases} \tag{2.19}$$

The pressure produced during atrial and ventricular contraction of the atrial / ventricular muscles then is modeled as

$$P_i(t) = E_{i,h}(t)\left(V_i(t) - V0_{i,h}\right), \tag{2.20}$$

where $V_i\left(t\right)$ is the volume in the vessel at time t and $V0_{i,h}$ is the void volume, the theoretical volume when there is no pressure generated in the heart [SSB07].

During relaxation, the pressure in each heart chamber was modeled using an exponential diastolic pressure-volume relationship [BS93]:

$$P_i(t) = e^{DS_{i,h}\cdot V_i(t)} - 1, \tag{2.21}$$

where $DS_{i,h}$ is the diastolic stiffness constant, and $V_i(t)$ is the volume of the heart chamber at time t.

The pressure of the atria and the right ventricle, $P_i(t)$ for $i = 1, 2, 3$, at any time is the maximum of equation (2.20) and equation (2.21). The flows for the atria are computed as shown in equation (2.10). This flow is the flow of blood into the atria at its entrance. Blood flow is not allowed to flow back into the right atrium from the right ventricle because the flow into the right ventricle is zero if the pressure difference between the right ventricle and right atrium is negative, as shown in equation (2.10). This emulates the tricuspid valve between the right atrium and right ventricle.

2.2.3 Modeling of the Aorta

The aorta is modeled as a standard blood vessel, with a modification for the inflow into the aorta due to the aortic valve between the right ventricle and aorta. This flow is defined as:

$$\max\{0, \frac{P_{RV}(t) - P_{AO}(t)}{R_{AO}}\}, \tag{2.22}$$

where P_{RV} and P_{AO} are the pressures of the right ventricle and aorta, respectively, and R_{AO} is the resistance of the aorta.

The aortic pressure is computed using two formulas. The first is the vessel pressure as a function of the vessel's volume and compliance (equation (2.33)). This determines the aortic pressure between ventricular contractions (diastole). During ventricular contraction (systole) the aortic pressure is identical to the ventricular pressure due to the opening of the valve (equation (2.30)). To create the needed inertia to pump blood through the modeled cardiovascular system, the aortic pressure (equation (2.35)) was substituted for all of the aorta vessel pressure (equation (2.33)). Switching between the two choices can be seen in Figure 2.3.

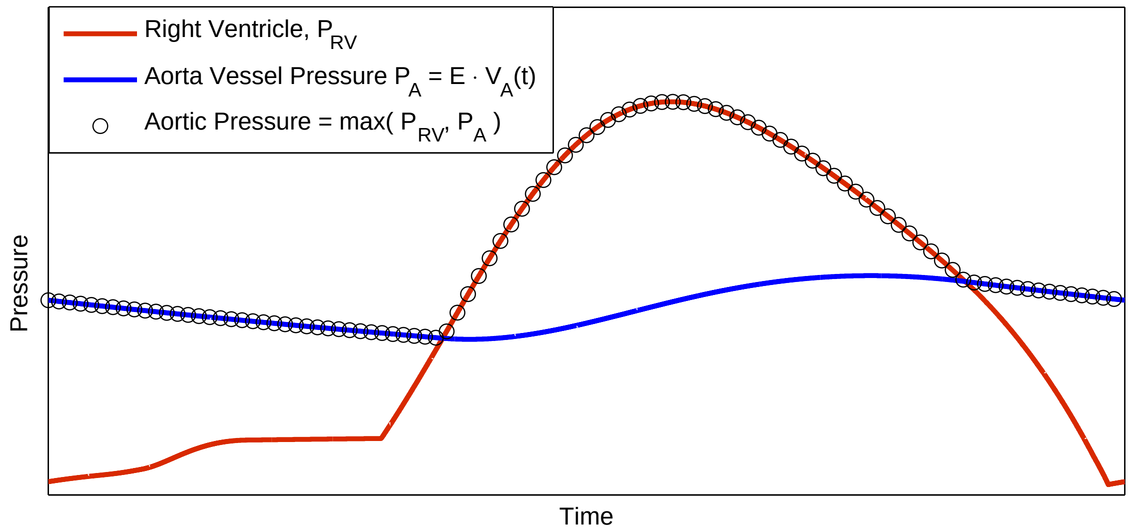

Figure 2.3: The figure shows pressure as a function of time for the right ventricle (red) and aorta (blue). The maximum pressure of the two, aortic pressure is denoted with the black circles.

2.3 Variable Notation

Table 2.1 shows the designations of the heart-related variables, while table 2.2 shows the designations of the variables in the other parts of the lumped circulatory system.

Table 2.1: Heart variable mappings

Description	Constants (R, C, E, E_{max})	Index for V, P, and Q
Left Atrium	$(1, h)$	1
Right Atrium	$(2, h)$	2
Right Ventricle	$(3, h)$	3

Table 2.2: Blood vessel variable mappings

Description	Constants (R, C, E)	Index for V, P, and Q
Aorta	$(1, s)$	4
Pulmonary Artery	$(2, s)$	5
Pulmonary Capillary	$(3, s)$	6
Pulmonary Vein	$(4, s)$	7
RV-PA Conduit or BT Shunt	$(5, s)$	8
Upper Systemic Capillaries	$(6, s)$	9
Superior Vena Cava	$(7, s)$	10
Lower Systemic Capillaries	$(8, s)$	11
Inferior Vena Cava	$(9, s)$	12

2.4 Right Ventricle-Pulmonary Arteries Model

The Right Ventricle-Pulmonary Arteries Conduit (RV-PA) model differs from the healthy heart, as the reconstructed aorta receives blood from the right ventricle, and a conduit connects the pulmonary arteries directly to the right ventricle. This is shown Figure 2.4.

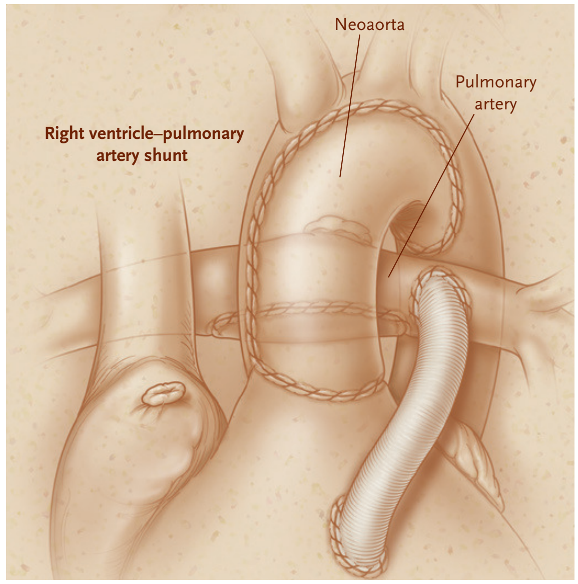

Figure 2.4: Illustration of the physiology of the Norwood procedure following the RV-PA conduit surgery. The reconstructed aorta connecting the right ventricle to the systemic cardiovascular system is labeled as the neoaorta. The RV-PA conduit is shown at the bottom right, reestablishing the connection between the ventricle and pulmonary circulation [OSM+10].

2.4.1 Equations

The block diagram of the construction of the RV-PA conduit cardiovascular system is shown in Figure 2.5. The system of ODEs used to model the volume of blood in each of the heart chambers and blood segments are shown below.

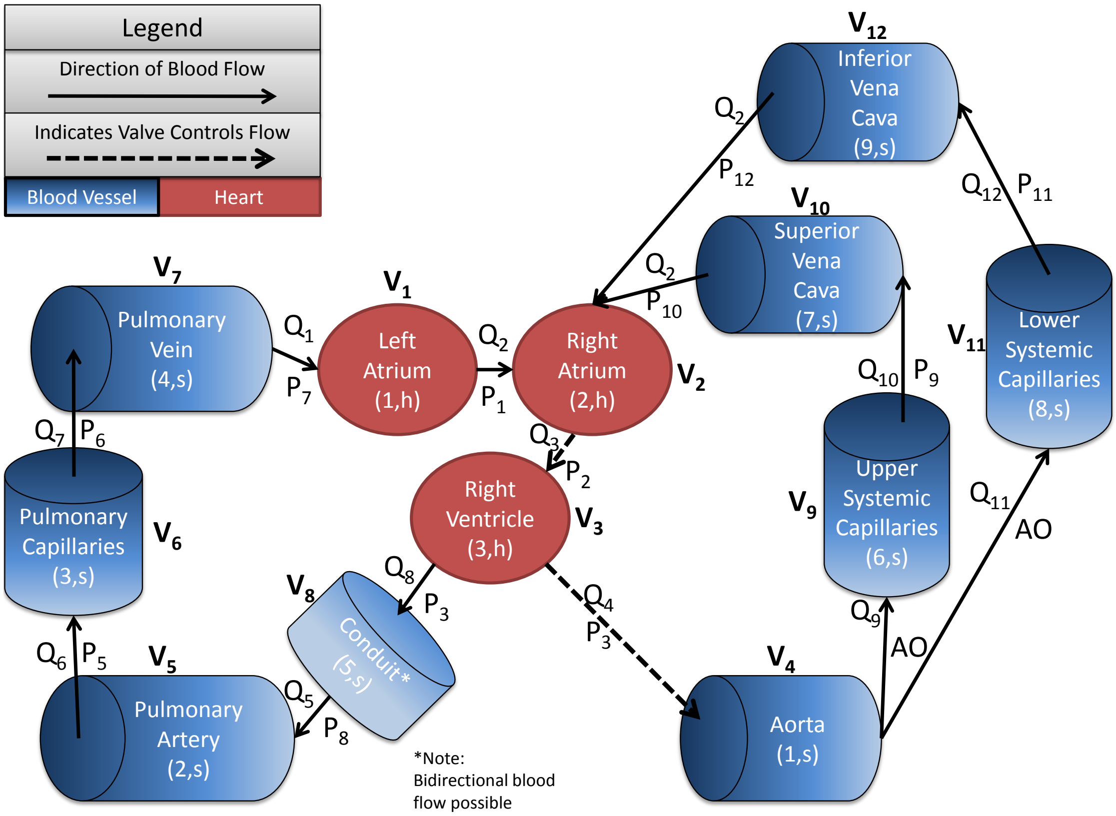

Figure 2.5: Block diagram of the compartment network used to model the RV-PA conduit cardiovascular system. The volume of each compartment is labeled by V_i, for $i = 1, \ldots, 12$. The line segments are labeled for the blood flow each represents, with the dashed lines representing flows between compartments regulated by valves. For example, Q_2 is the blood flow into the right atrium and is represented by lines from its three different sources. Similarly, all line segments are labeled for which pressures they represent. The aortic pressure AO is used multiple times in the model.

Left Atrium, 1 / (1,h)

$$\dot{V}_1(t) = Q_1(t) - \frac{P_1(t) - P_2(t)}{R_{2,h}} \tag{2.23}$$

$$P_1\,(t) = \max\{e^{\left(DS_{1,h}\cdot V_1(t)\right)} - 1, E_{1,h}\,(t)\,(V_1\,(t) - V0_{1,h})\} \tag{2.24}$$

$$Q_1\,(t) = \frac{P_7\,(t) - P_1\,(t)}{R_{1,h}}, \tag{2.25}$$

Right Atrium, 2 / (2,h)

$$\dot{V}_2(t) = Q_2(t) - Q_3(t) \tag{2.26}$$

$$P_2\left(t\right) = \max\{e^{\left(DS_{2,h}\cdot V_2(t)\right)} - 1, E_{2,h}\left(t\right)\left(V_2\left(t\right) - V0_{2,h}\right)\} \tag{2.27}$$

$$Q_2\left(t\right) = \frac{P_1(t) - P_2(t)}{R_{2,h}} + \frac{P_{10}(t) - P_2(t)}{R_{SVC}} + \frac{P_{12}(t) - P_2(t)}{R_{IVC}}, \tag{2.28}$$

Right Ventricle, 3 / (3,h)

$$\dot{V}_3(t) = Q_3(t) - \left(Q_4(t) + Q_8(t)\right) \tag{2.29}$$

$$P_3\left(t\right) = \max\{e^{\left(DS_{3,h}\cdot V_3(t)\right)} - 1, E_{3,h}\left(t\right)\left(V_3\left(t\right) - V0_{3,h}\right)\} \tag{2.30}$$

$$Q_3\left(t\right) = \max\{0, \frac{P_2\left(t\right) - P_3\left(t\right)}{R_{3,h}}\} \tag{2.31}$$

Aorta, 4 / (1,s)

$$\dot{V}_4(t) = Q_4(t) - \left(Q_9(t) + Q_{11}(t)\right) \tag{2.32}$$

$$P_4\left(t\right) = V_4\left(t\right) E_{1,s} \tag{2.33}$$

$$Q_4\left(t\right) = \max\{0, \frac{P_3\left(t\right) - P_4\left(t\right)}{R_{1,s}}\} \tag{2.34}$$

$$A0\left(t\right) = \max\{P_3\left(t\right), P_4\left(t\right)\} \tag{2.35}$$

Pulmonary Artery, 5 / (2,s)

$$\dot{V}_5(t) = Q_5(t) - Q_6(t) \tag{2.36}$$

$$P_5\left(t\right) = V_5\left(t\right) E_{2,s} \tag{2.37}$$

$$Q_5\left(t\right) = \frac{P_8\left(t\right) - P_5\left(t\right)}{R_{2,s}} \tag{2.38}$$

Pulmonary Capillaries, 6 / (3,s)

$$\dot{V}_6(t) = Q_6(t) - Q_7(t) \tag{2.39}$$

$$P_6\,(t) = V_6\,(t)\,E_{3,s} \tag{2.40}$$

$$Q_6\,(t) = \frac{P_5\,(t) - P_6\,(t)}{R_{3,s}} \tag{2.41}$$

Pulmonary Vein, 7 / (4,s)

$$\dot{V}_7(t) = Q_7(t) - Q_1(t) \tag{2.42}$$

$$P_7\,(t) = V_7\,(t)\,E_{4,s} \tag{2.43}$$

$$Q_7\,(t) = \frac{P_6\,(t) - P_7\,(t)}{R_{4,s}} \tag{2.44}$$

Conduit, 8 / (5,s)

$$\dot{V}_8(t) = Q_8(t) - Q_5(t) \tag{2.45}$$

$$P_8\,(t) = V_8\,(t)\,E_{5,s} \tag{2.46}$$

$$Q_8\,(t) = \frac{P_3\,(t) - P_8\,(t)}{R_{5,s}} \tag{2.47}$$

Upper Systemic Capillaries, 9 / (6,s)

$$\dot{V}_9(t) = Q_9(t) - Q_{10}(t) \tag{2.48}$$

$$P_9\,(t) = V_9\,(t)\,E_{6,s} \tag{2.49}$$

$$Q_9\,(t) = \frac{A0\,(t) - P_9\,(t)}{R_{6,s}} \tag{2.50}$$

Superior Vena Cava, 10 / (7,s)

$$\dot{V}_{10}(t) = Q_{10}(t) - \frac{P_{10}(t) - P_2(t)}{R_{SVC}} \tag{2.51}$$

$$P_{10}(t) = V_{10}(t)\, E_{7,s} \tag{2.52}$$

$$Q_{10}(t) = \frac{P_9(t) - P_{10}(t)}{R_{7,s}} \tag{2.53}$$

Lower Systemic Capillaries, 11 / (8,s)

$$\dot{V}_{11}(t) = Q_{11}(t) - Q_{12}(t) \tag{2.54}$$

$$P_{11}(t) = V_{11}(t)\, E_{8,s} \tag{2.55}$$

$$Q_{11}(t) = \frac{A0(t) - P_{11}(t)}{R_{8,s}} \tag{2.56}$$

Inferior Vena Cava, 12 / (9,s)

$$\dot{V}_{12}(t) = Q_{12}(t) - \frac{P_{12}(t) - P_2(t)}{R_{IVC}} \tag{2.57}$$

$$P_{12}(t) = V_{12}(t)\, E_{9,s} \tag{2.58}$$

$$Q_{12}(t) = \frac{P_{11}(t) - P_{12}(t)}{R_{9,s}} \tag{2.59}$$

2.5 Blalock Taussig Shunt Model

The Blalock Taussig (BT) shunt model differs from the RV-PA conduit model in that instead of the conduit coming from the right ventricle to connect the pulmonary system, an artery from the aorta is connected to the pulmonary system. This is shown in Figure 2.6.

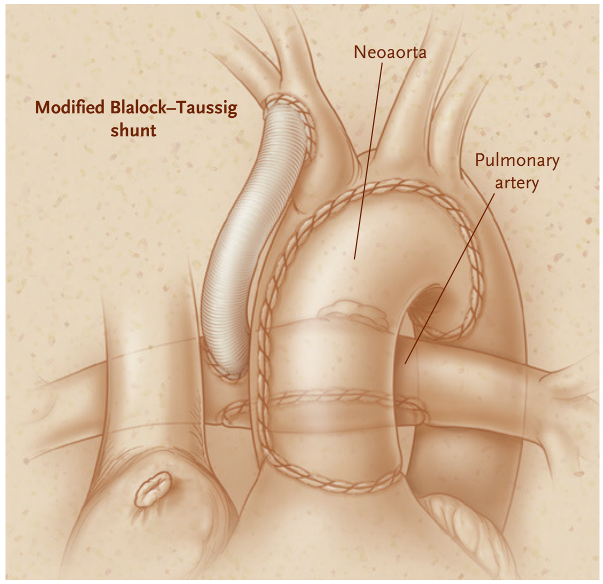

Figure 2.6: Illustration of the physiology of the Norwood procedure following the BT shunt surgery. The reconstructed aorta connecting the right ventricle to the systemic cardiovascular system is labeled as the neoaorta. The shunt is shown at the top middle, establishing the connection between the reconstructed aorta and pulmonary circulation [OSM+10].

2.5.1 Equations

The system of ODEs used to model blood volume in each of the heart chambers and blood segments represented in Figure 2.7 is very similar to those used to model the RV-PA conduit. Equations (2.60)-(2.62) are the only differences between these models. The block diagram showing the construction of the BT shunt cardiovascular system is shown in Figure 2.7.

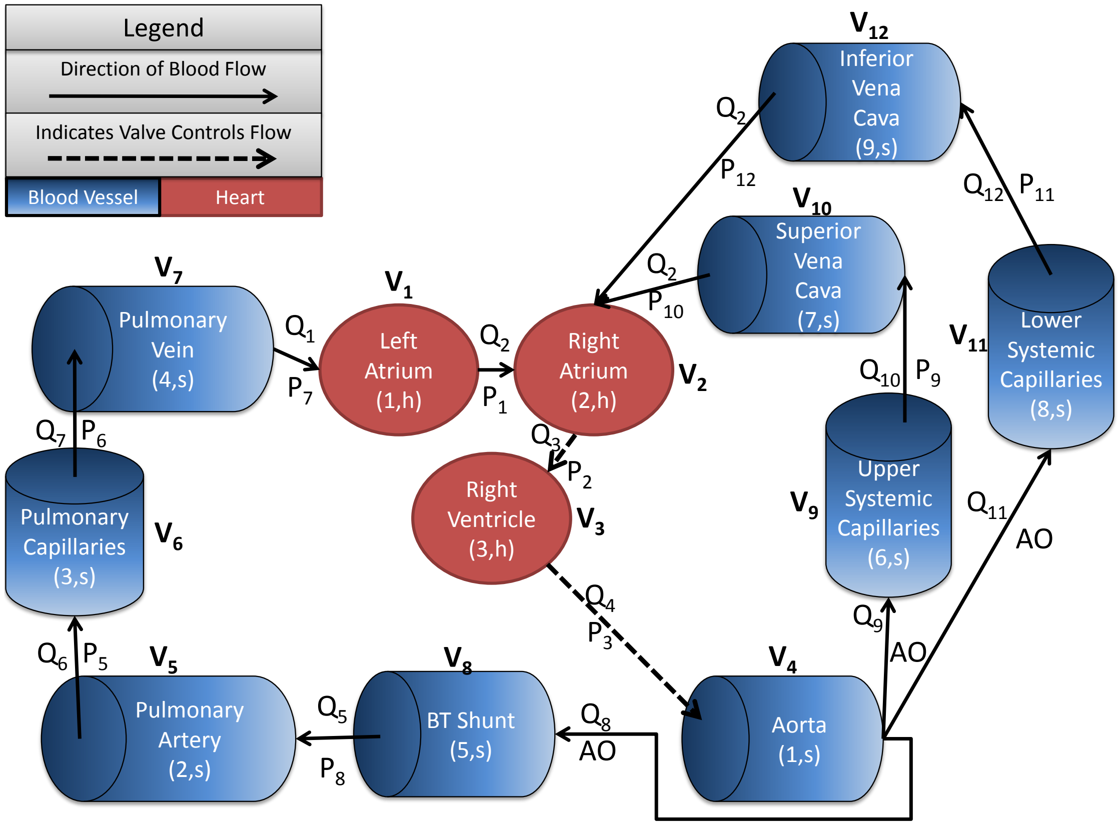

Figure 2.7: Block diagram of the compartment network used to model the BT shunt cardiovascular system. The volume of each compartment is labeled by V_i, for $i = 1, \ldots, 12$. The line segments are labeled for the blood flow each represents, with the dashed lines representing flows between compartments regulated by valves.

Right Ventricle

$$\dot{V}_3(t) = Q_3(t) - Q_4(t) \tag{2.60}$$

Aorta, 4 / (1,s)

$$\dot{V}_4(t) = Q_4(t) - (Q_8(t) + Q_9(t) + Q_{11}(t)) \tag{2.61}$$

BT Shunt, 8 / (5,s)

$$Q_8\left(t\right) = \frac{AO\left(t\right) - P_8\left(t\right)}{R_{5,s}} \tag{2.62}$$

Chapter 3

COMPUTER IMPLEMENTATION DETAILS

The implementation of the model was done in MATLAB R2010a (Student Version) and consists of three parts:

- Simulation Core: Module performing the simulation of the cardiovascular system
- GUI: User interface to modify key parameters
- Parameter Searching: Module used to find the set of parameters that creates the best match to a desired P-V loop.

3.1 Simulation Core

Figure 3.1 illustrates the simulation core explained in this section. Each heart chamber and blood vessel utilizes various constants representing resistances, compliances, etc. These cardiovascular system parameters are maintained in two structures. One structure was created to store $R_{i,h}$, $E_{i,max}$, $DS_{i,h}$, and $V0_{i,h}$ for $i = 1, 2, 3$. For the blood vessels, a second structure was created to store $E_{i,s}$ and $R_{i,s}$ for $i = 1, \ldots, 9$. These structures containing the constants are set before the simulation is executed.

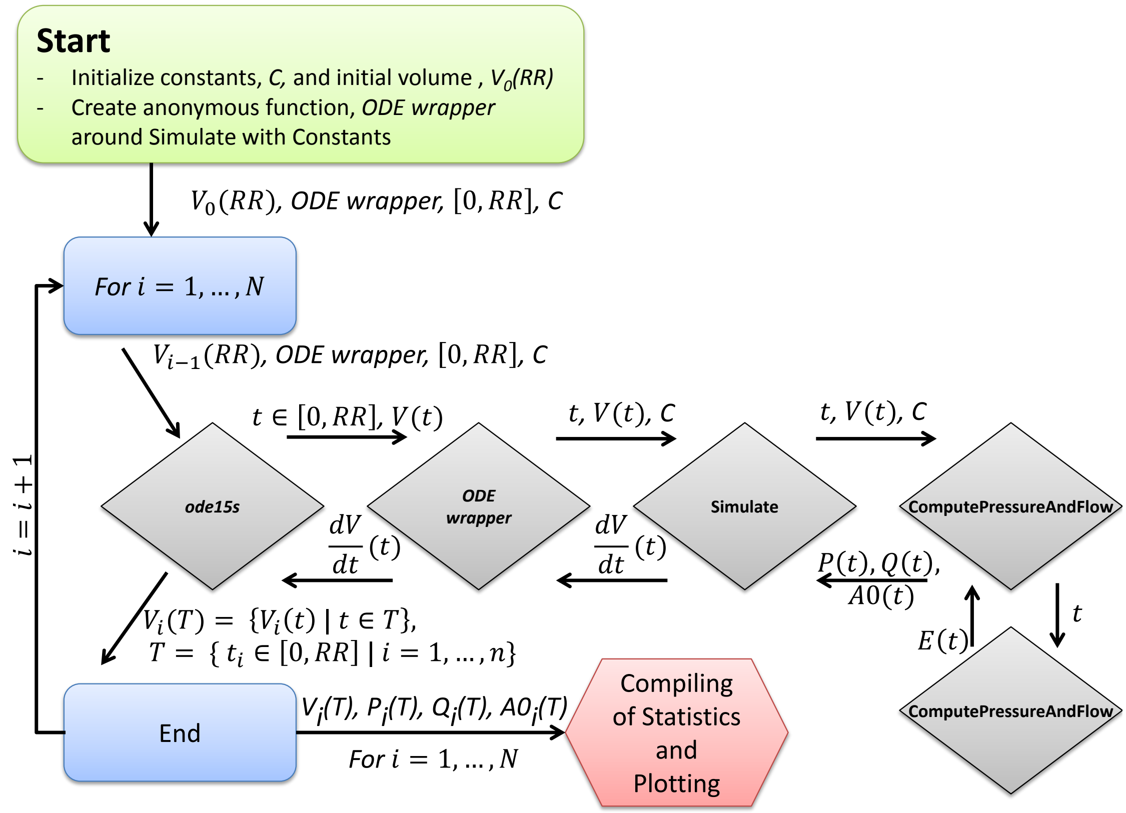

Figure 3.1: Simulation of the cardiovascular system

A uniform partition of n time elements over the interval $[0, RR]$,

$$T = \{t_i = \left(\frac{i}{n}\right) \cdot RR \mid i = 1, \dots, n\},$$

is created by the simulation core. The results of each iteration for V, P, and Q are matrices in $\mathbb{R}^{n \times 12}$ and represent the volumes, pressures, and flows of the cardiovascular system at each time $t_i \in T$. (i.e. the m^{th} entry in the 3^{rd} column of V is $V_3(t_m)$ for some $m = 1, \dots, n$.).

The simulation core consists of functions to initialize heart chamber and blood vessel parameters, compute contractility of the heart chambers and elastance of the blood vessels, compute pressure and flow of each compartment, and calculate $\frac{dV}{dt}$ for each chamber. The first function executed initializes the structures containing the circulatory parameters, RR, STI, and initial volumes, $V_0(RR) \in \mathbb{R}^{12}_{+}$. Also among the constants is a flag representing whether the model is to reflect a RV-PA conduit cardiovascular system or a BT-shunt cardiovascular system.

The system of ODEs (equations (2.23)-(2.62)) is solved as an initial value problem (IVP) using the MATLAB solver `ode15s`. This solver was chosen due to the existence of the maximum functions, representing the valves (tricuspid and aortic valves). These discontinuities make the system of ODEs numerically stiff. The IVP solver `ode15s` requires a MATLAB function that returns $\frac{dV}{dt} \in \mathbb{R}^{12}$ when given a time, $t \in [0, RR]$ and corresponding volumes, $V \in \mathbb{R}^{12}$ of all the blood vessels and heart chambers as arguments. This function is called `Simulate`. As an intermediate step, it computes the corresponding pressures and flows of each compartment.

`Simulate` utilizes the function `ComputePressureAndFlow`, which is passed the same arguments. `ComputePressureAndFlow` returns the pressures and flow of each compartment and aortic pressure for an $n \times 1$ vector of times ($n = 1$ when `Simulation` is making the function call), $P, Q \in \mathbb{R}^{n\times 12}$, $AO \in \mathbb{R}^n$, respectively. The function also makes a call to `ComputeContractility` which computes the contractility $E \in \mathbb{R}^{n\times 13}$ for each heart chamber and returns the constant compliances of the blood vessels for each time.

The solution returned by the ODE solver represents the computed volumes of each of the compartments for the given time span for one cycle of a heartbeat. Because we do not have an accurate feasible initial condition for the entire system, the solver is iterated in a `for` loop to run for N cycles. The number of heartbeats needed is large enough such that given the initial volume of each compartment, $V_0(RR) \in \mathbb{R}^n$, the solution converges to a limit cycle. For the first time through the loop, the initial volume $V_0(RR)$ is passed to the simulation function. For the i^{th} iteration, $1 < i \leq N$, the initial volume is then set to $V_{i-1}(RR)$, the volume of the vessels in the previous iteration at the last time point. Figure 3.2 illustrates the convergence of the solutions to a stable limit cycle.

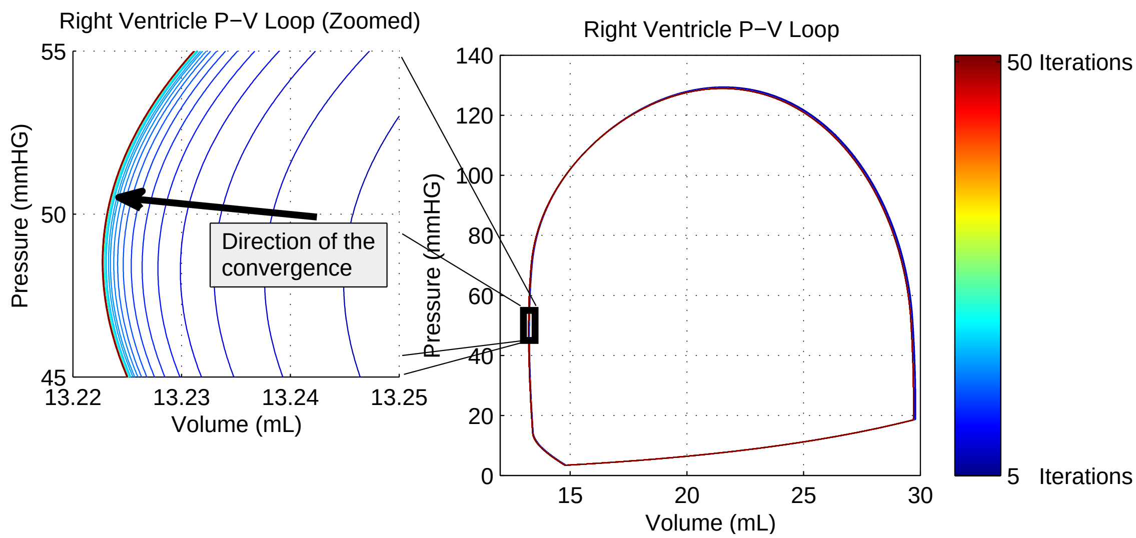

Figure 3.2: The figure on the right shows the resultant P-V loop of the right ventricle from each iteration on the same plot. Each iteration is representative of a heartbeat. The figure on the left is a zoomed in section of the figure on the right. The direction of the convergence is shown with an arrow.

3.2 GUI

A GUI was built around the simulation core to provide a means for the user to select a subset of parameters values. Initial values of the parameters were chosen for the user to change through the interface. The layout of the available parameters and the editable fields in the GUI are shown in Figure 3.3.

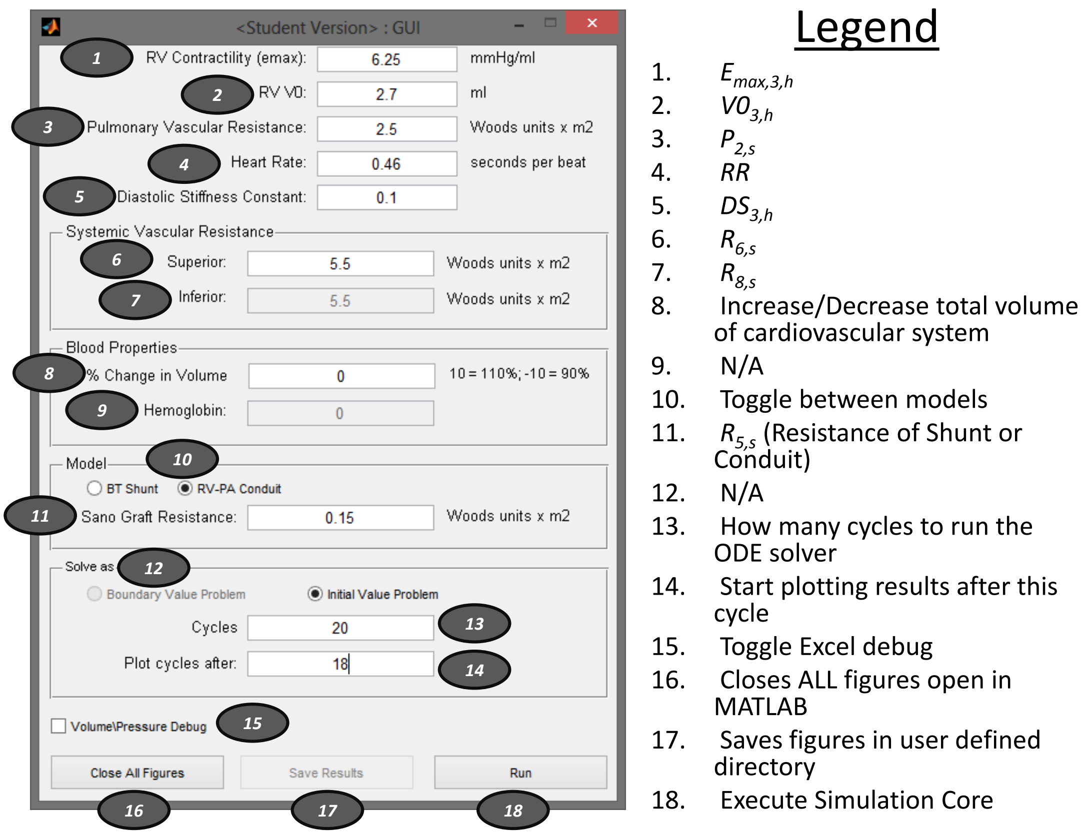

Figure 3.3: GUI screenshot

When the simulation is executed through the GUI, the data from the cycles given in the edit box 14 to edit box 13 of Figure 3.3 will be shown in the generated plots shown in Figure 3.4. Moreover, the number of iterations N is set in box 13.

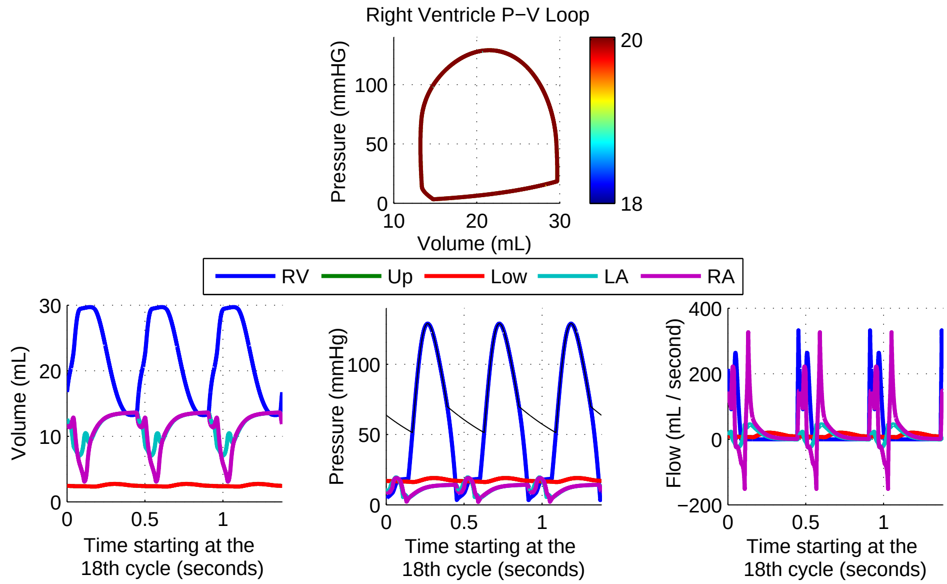

Figure 3.4: Sample graphical output from the GUI. The top figure of Figure 3.4 is the generated P-V loop from the execution of the simulation. The bottom three figures are volume vs. time (bottom left), pressure vs. time (bottom center), and flow vs. time (bottom right) of the right ventricle, upper and lower systemic capillaries, and left and right atria.

3.3 Parameter Identification

The initial set of parameters utilized in the GUI did not produce a fully realistic P-V loop. At the least, a P-V loop for HLHS patients should have minimum and maximum volume of 15 mL and 30 mL, respectively. It also should have minimum and maximum pressure of 5 mmHg and 80 mmHg, respectively. Adjusting the parameters manually to produce a fully realistic P-V loop is a rather daunting task due to the dimension of the solution space. There are 30 parameters in the model, each having global effects on the behavior of the cardiovascular system. Rather than tune the model by hand, a least-squares optimizer was utilized. The MATLAB function `lsqnonlin` solves nonlinear least-squares problems expressed as

$$\min ||f(x)||_2^2 = \min \left(f_1(x)^2 + f_2(x)^2 + \cdots + f_n(x)^2\right).$$

To express the parameter searching problem as a nonlinear least-squares problem, an objective function was defined to map a set of parameters representing the constants of the model at the j^{th} iteration, x_j to a vector of residuals

$$[f_1(x_j), f_2(x_j), \ldots, f_n(x_j)]$$

for some $n > 0$. The objective function defines a uniform partition of the interval $[0, RR]$, $T = \{t_i \in T \mid i = 1, \ldots, |T|\}$. A uniform partition of 100 elements was used for our results. Given the volume and pressure of the theoretical P-V loop with the desired traits and the P-V loop corresponding to the given values over this partition T, the objective residual is defined as

$$f_i(x_j) = \sqrt{(V_{3,h}(t_i) - V_{obj}(t_i))^2 + (P_{3,h}(t_i) - P_{obj}(t_i))^2}, \quad t_i \in T,$$

where $V_{3,h}, P_{3,h}$ are the volume and pressures associated with the constants x_j and V_{obj}, P_{obj} are the corresponding volume and pressure on the goal P-V loop.

Figure 3.5 illustrates how the objective function is evaluated for a partition of 100 points (i.e. $|T| = 100$ and $t_i = i \cdot \frac{RR}{100}$ for $i = 1, \ldots, 100$). The left hand side figure shows the P-V loop of the goal (blue) and the current parameters being evaluated (red). The lengths of the black lines are representative of the $f_i(x)$'s for $i = 1, \ldots, 100$, where the points shown in the figure are the corresponding points in time. The two figures on the right show volume versus time (top right) and pressure versus time (bottom right) corresponding to the goal P-V loop (blue) and the current P-V loop being evaluated (red). The black lines of the figures on the right illustrate the differences between volumes and pressures. The squared residual of the objective function is an approximately scaled sum of the squares of the areas between the curve pairs.

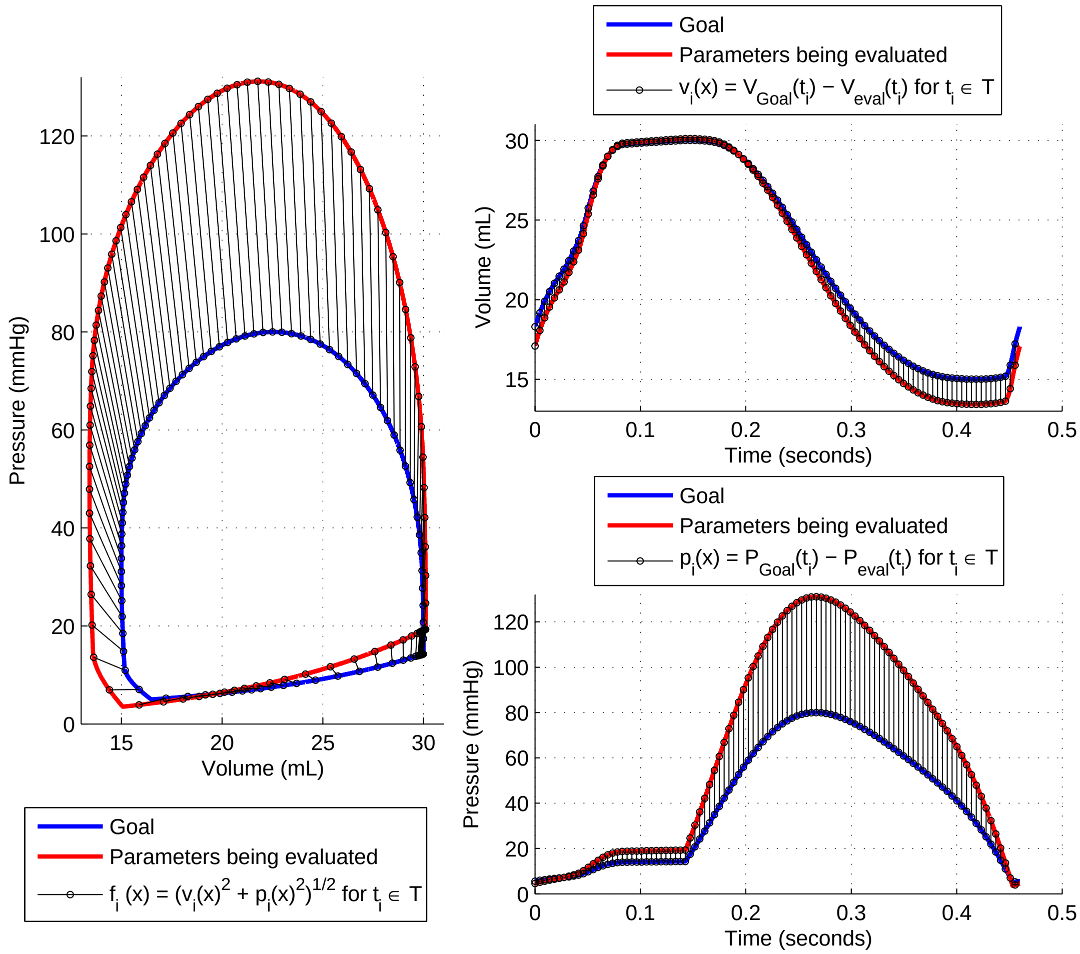

Figure 3.5: Evaluation of objective junction example for $|T| = 100$. The figure on the left shows the P-V loop evaluated from the current parameters in blue and the goal P-V loop in red. The black lines show the sampled differences between the two P-V loops. The figures on the right show the corresponding volumes (top) and pressures (bottom) vs. time. The black lines on each plot are the sampled differences between the volumes and pressures.

To derive a goal P-V loop, a linear transformation was applied to the P-V loop of the right ventricle from the RV-PA model utilizing the default GUI constants (Figure 3.4). In Figure 3.6, the P-V loops corresponding to the original GUI parameters for the RV-PA conduit model (green) and BT shunt (blue) are shown with the derived goal P-V loop (red).

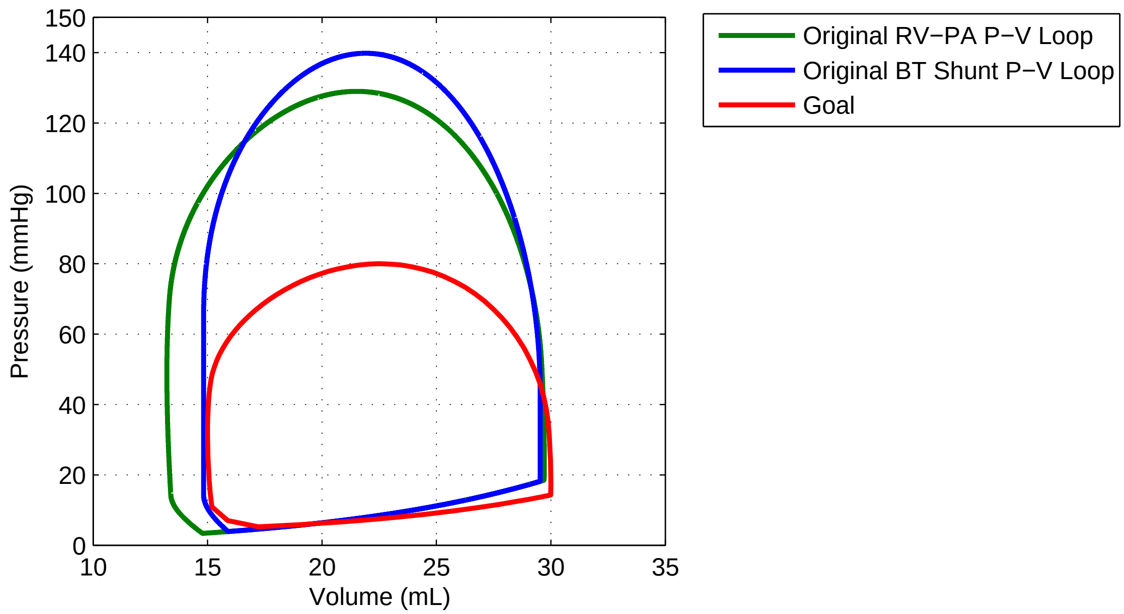

Figure 3.6: The goal P-V loop is shown in is shwon in red with the RV-PA conduit and BT shunt evaluated with the initial parameters shown in green and blue, respectively.

The flow of the code for the parameter identification is shown in Figure 3.7. Similar to the simulation core, the start of the program sets the initial values of the parameters and volumes at RR, $V_0(RR)$. The initialization also defines which parameters to pass the optimizer `lsqnonlin`. The program then defines an anonymous function used to wrap the objective function, passing it the initial parameters, which parameters are being optimized by `lsqnonlin`, the partition of $[0, RR]$, T, and the goal volume and pressure evaluated over T, V_{obj} and P_{obj}, respectively.

The start of the program then gives `lsqnonlin` an initial guess for the parameters being tuned in the form of a vector x_0 and the anonymous function handle to the objective function. When `lsqnonlin` calls the objective function, it passes the current estimate of the parameters being tuned, x_j. The objective function wrapper augments these with the set of fixed parameters to enable calling the simulation core (Figure 3.1). The simulation core is then executed, returning a set of simulated volumes and pressures of the cardiovascular system evaluated over the partition T. The objective function then computes $\{f_i(x_j) \mid i = 1, \ldots, |T|\}$ and returns this vector to the optimizer.

Once any of the stopping conditions are reached by `lsqnonlin`, such as finding the solution, maximum number of iterations being executed, or minimum step size of the solution reached, the last computed solution x_M and the reason for stopping are returned. Figure 3.8 shows an example of the results of the parameter identification code.

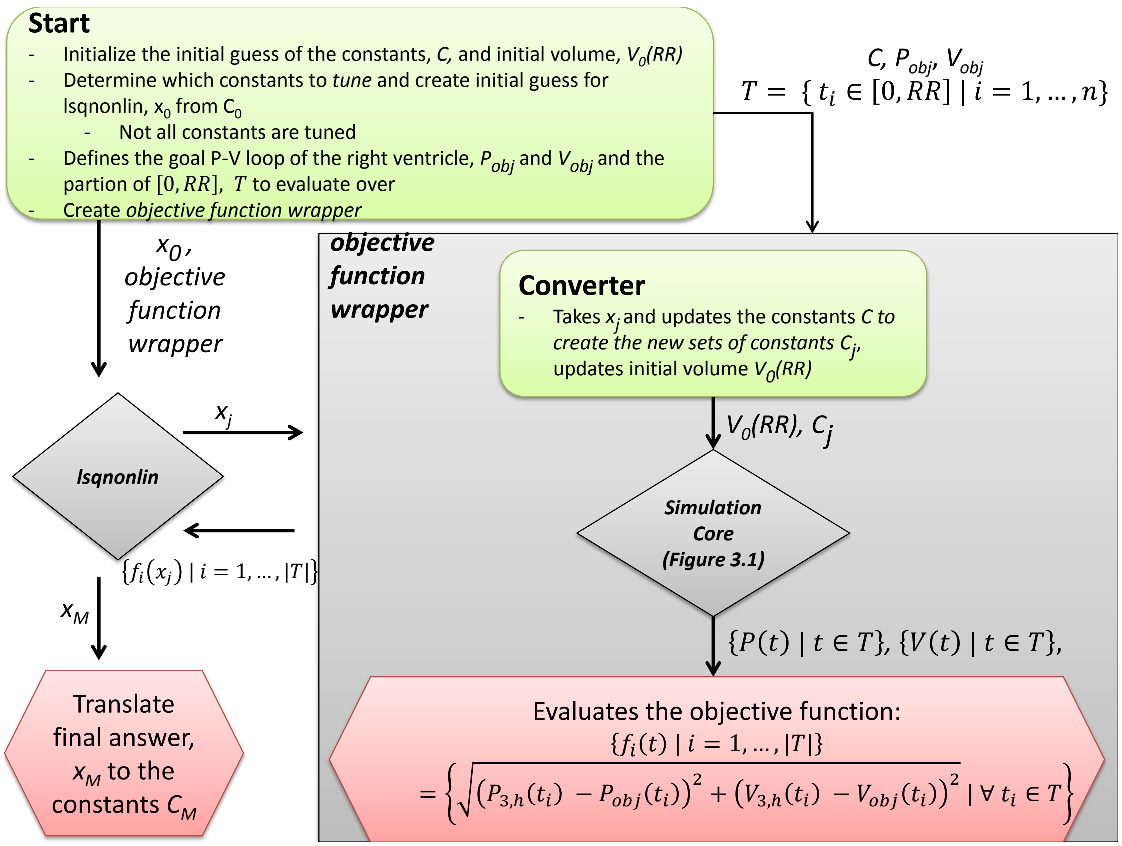

Figure 3.7: Flow chart of paramater search

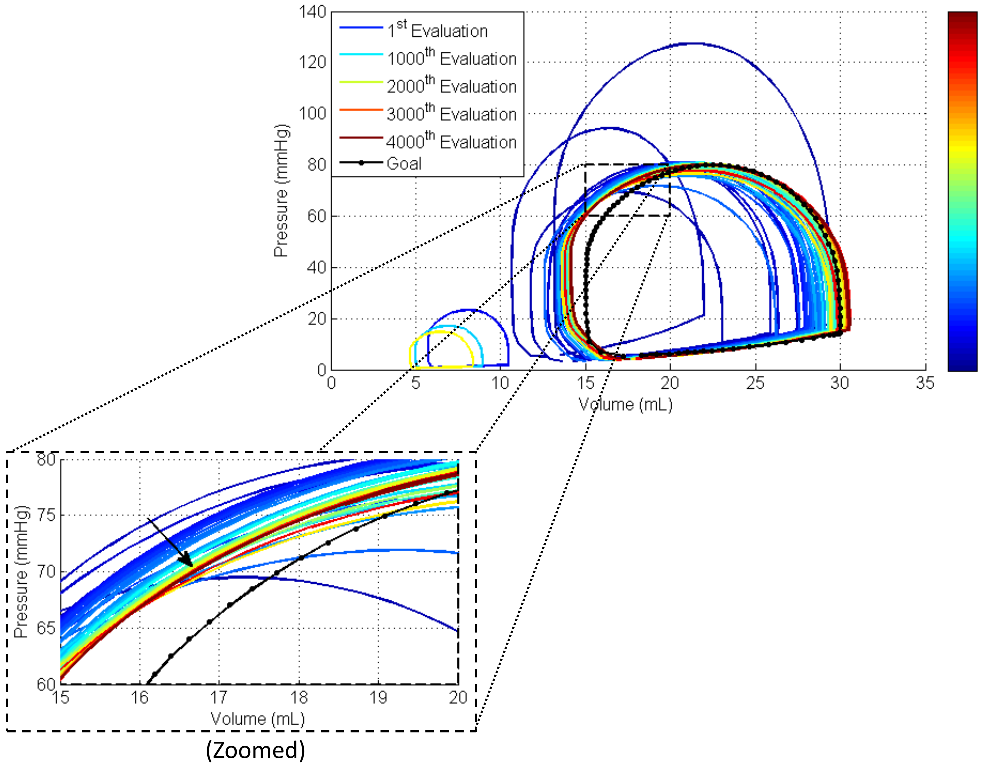

Figure 3.8: Example of parameter identification. The initial estimate of the first evaluation is shown in blue and is the P-V loop with the largest pressure in the top right figure. The iterations are colored from blue (first estimate of the solver) to dark red (the last estimate of the solver). The P-V loops can be seen moving towards the objective P-V loop, shown in black in both figures. This is further illustrated in the bottom left figure showing a zoomed in portion of the upper right plot.

Chapter 4

RESULTS

The resulting parameters utilizing the ventricular P-V loop for both the RV-PA conduit model and BT shunt model were evaluated to determine which physiology effects were captured well and which were not. The optimizer was allowed to modify all resistances of each blood vessel and heart chamber, $R_{i,h}$ and $R_{j,s}$ for $i = 1, 2, 3$ and $j = 1, \ldots, 7$ and the elastances of each blood vessel, $E_{j,s}$ for $j = 1, \ldots, 7$. The resistances of each blood vessel flowing into the atria, $R_{1,h}, R_{IVC}$ and R_{SVC} were related so that the optimizer treated them as one parameter, i.e. $R_{1,h} = R_{IVC} = R_{SVC}$. Symmetry assumptions about the physiology led to additional equalities:

- The resistances of the lower and upper systemic capillaries, $R_{6,s} = R_{8,s}$.
- The elastances of the lower and upper systemic capillaries, $E_{6,s} = E_{8,s}$.
- The resistances of the inferior vena cava and superior vena cava, $R_{7,s} = R_{9,s}$
- The elastances between the capillaries and their respective vena cava, $E_{7,s} = E_{9,s}$

The $E_{max,i,h}$ of each heart chamber was allowed to be modified, $i = 1, 2, 3$. The diastolic stiffnesses of the atria, $DS_{1,h}$ and $DS_{2,h}$ were also variables subject to $DS_{1,h} = DS_{2,h}$. Finally, the initial volume of blood in each compartment was also scaled by the same proportion controlled by the optimizer.

4.1 RV-PA Conduit Resulting Parameters

Figure 4.1 shows the resulting RV-PA conduit P-V loop obtained by optimization compared to the goal P-V loop. It is important to note that the optimizer reached the maximum number of objective function evaluations. Due to the diminishing returns observed in the behavior of the optimizer towards the end of the run, the parameter values were taken as nearly optimized, at least locally.

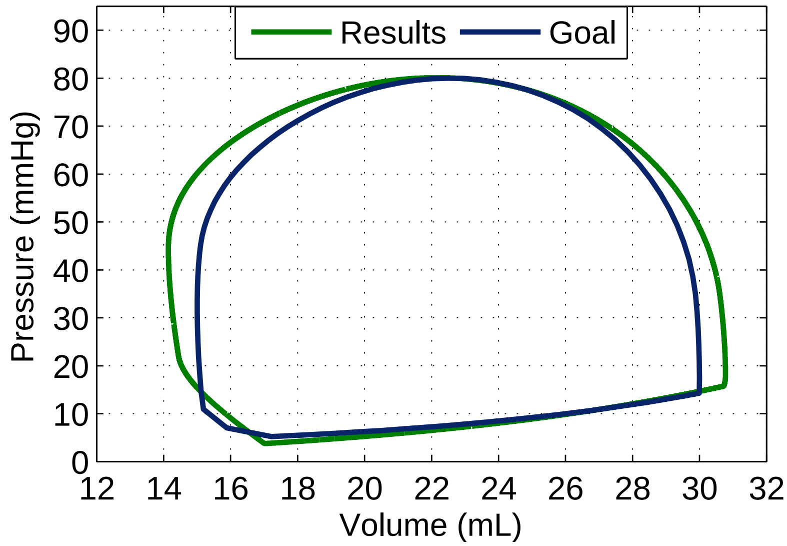

Figure 4.1: Resulting P-V loop of the RV-PA conduit model. The goal P-V loop is shown in blue, and the resulting P-V loop from the optimizer in green.

While the resulting simulation does not perfectly match the goal P-V loop, it has several desirable characteristics. The ventricular stroke volume of 16.6 mL is appropriate. The resulting ventricular pressures were also in a reasonable range of 3.8 mmHg to 80.1 mmHg. As we expected, the resulting P-V loop also shows a very limited IVCT. Rather than observing a vertical line from the bottom right corner of the loop to the top right, a rounded corner is noted. This was expected and due to the lower blood pressure of the pulmonary system (Figure 4.4) when compared to that of the right ventricle (Figure 4.2). This lower blood pressure is creating a pressure head from the right ventricle, into the valveless RV-PA conduit, and into the pulmonary artery. The declined IVRT (as compared to a healthy heart) is also in line with expectations for the RV-PA heart.

The resultant P-V loop in Figure 4.1 does show an unexpected corner cut-off at the bottom left (end of IVRT). While back-flow causing an early increase of volume at the end IVRT is attributed to the lack of valve between the pulmonary system and right ventricle in the model, this may be too large to be realistic for the RV-PA conduit. The pressures of the the three heart chambers (middle plot of Figure 4.2) show a sharp drop in the right ventricular pressure. This pressure drops lower than that of the right atrium, causing the blood to flow from the atria into the right ventricle and the observed behavior of this corner.

Figures 4.2 to 4.4 show the volumes (top figure), pressures (middle figure) and flow (bottom figure) versus time for the heart, systemic system, and pulmonary system, respectively. Upon further inspection, the limited IVCT is not entirely due to the valveless RV-PA conduit. The lower blood pressure of the systemic components is causing low blood pressure in the aorta and causing the aortic valve to open perhaps earlier than it should. Also note that there is observed back-flow from the right atrium into the left atrium. This is caused by a small pressure difference between the two atria and a very small resistance of the right atrium, $R_{2,h}$ (Table 4.1).

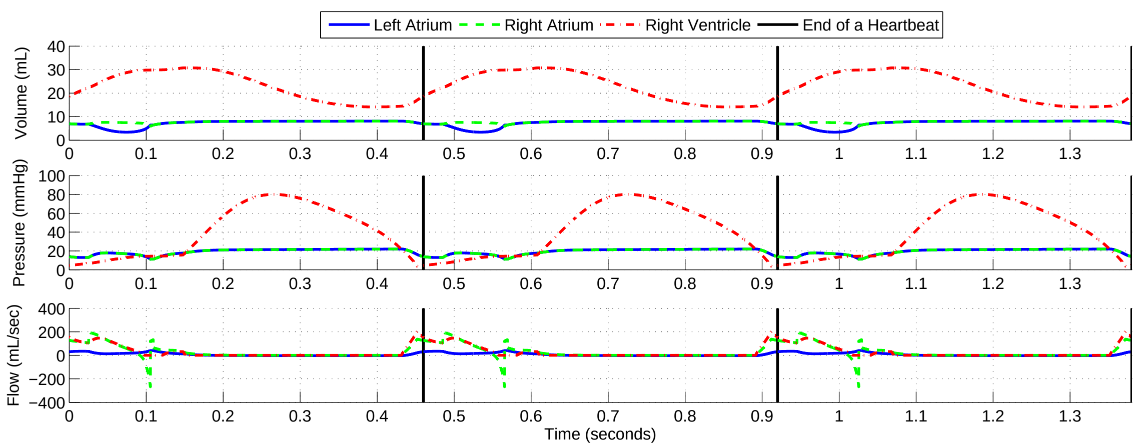

Figure 4.2: Volume, pressure, and flow of the heart vs. time of the RV-PA model. In all three figures the left atrium is shown in blue solid line, the right atrium in green dashed line, and right ventricle in the red dashed-dot line. Each heartbeat is delineated by a solid black line. The top plot is the volume vs. time, middle plot is pressure vs. time, and the bottom plot is the flow vs. time.

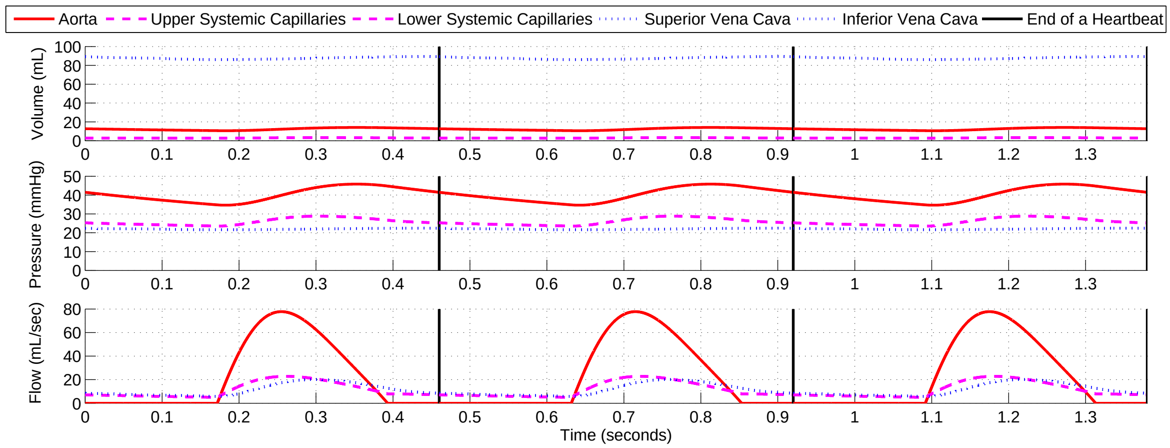

Figure 4.3: Volume, pressure, and flow of the systemic system vs. time of the RV-PA model. In all three figures the aorta is shown in the red solid line, the upper and lower systemic capillaries in the pink dashed line, and superior and inferior vena cavas in the blue dotted line. Each heartbeat is delineated by a solid black line. The top plot is the volume vs. time, middle plot is pressure vs. time, and the bottom plot is the flow vs. time.

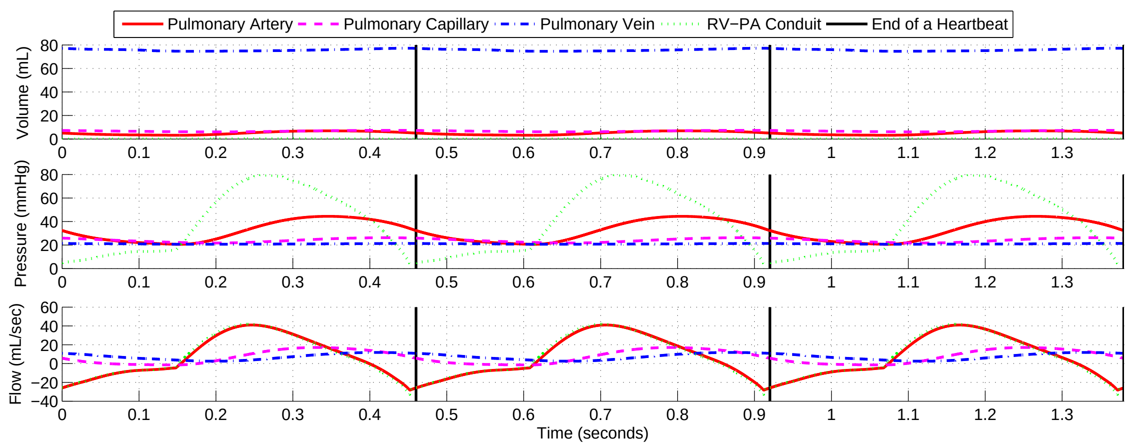

Figure 4.4: Volume, pressure, and flow of the pulmonary system vs. time of the RV-PA model. In all three figures the pulmonary artery is shown in the red solid line, the pulmonary capillary in the pink dashed line, pulmonary vein in the blue dashed-dotted line, and the RV-PA conduit in the green dotted line. Each heartbeat is delineated by a solid black line. The top plot is the volume vs. time, middle plot is pressure vs. time, and the bottom plot is the flow vs. time.

The optimized parameters and their original values are shown in tables 4.1 and

4.2 for the heart and blood vessels, respectively. In table 4.2, the reason for the low systemic blood pressure can be seen. The aorta was made to be more compliant than the pulmonary artery with a small resistance. The compliance of the aorta should be less than or equal to the compliance of the pulmonary artery. Similarly, the resistance of the aorta should be comparable to the resistance of the pulmonary artery.

Table 4.1: Optimized RV-PA conduit heart parameters

Description	Parameter	Original	Optimized
Resistance			
Left Atrium	$R_{1,h}$	0.198	0.241
Right Atrium (from Left Atrium)	$R_{2,h}$	0.018	4.1e-7
Right Atrium (from Lower Systemic)	R_{IVC}	0.198	0.241
Right Atrium (from Upper Systemic)	R_{SVC}	0.198	0.241
Right Ventricle	$R_{3,h}$	0.047	0.062
E_{max}			
Left Atrium	$E_{max,1,h}$	4.026	3.762
Right Atrium	$E_{max,2,h}$	1.884	1.546
Right Ventricle	$E_{max,3,h}$	3.773	3.758
Diastolic Stiffness			
Left Atrium	$DS_{1,h}$	0.432	0.388
Right Atrium	$DS_{2,h}$	0.432	0.388
Right Ventricle	$DS_{3,h}$	0.092	0.092

Table 4.2: Optimized RV-PA conduit blood vessel parameters

Description	Parameters	Original	Optimized
Resistance			
Aorta	$R_{1,s}$	0.495	0.510
Pulmonary Artery	$R_{2,s}$	1.172	1.056
Pulmonary Capillaries	$R_{3,s}$	0.968	1.133
Pulmonary Vein	$R_{4,s}$	0.415	0.415
RV-PA Conduit	$R_{5,s}$	0.003	0.019
Upper Systemic Capillaries	$R_{6,s}$	2.493	2.280
Superior Vena Cava	$R_{7,s}$	0.354	0.339
Lower Systemic Capillaries	$R_{8,s}$	2.493	2.280
Inferior Vena Cava	$R_{9,s}$	0.354	0.339
Inverse compliance			
Aorta	$E_{1,s}$	3.174	3.257
Pulmonary Artery	$E_{2,s}$	6.512	6.402
Pulmonary Capillaries	$E_{3,s}$	3.220	3.573
Pulmonary Vein	$E_{4,s}$	0.274	0.277
RV-PA Conduit	$E_{5,s}$	278.394	254.322
Upper Systemic Capillaries	$E_{6,s}$	8.553	8.781
Superior Vena Cava	$E_{7,s}$	0.238	0.251
Lower Systemic Capillaries	$E_{8,s}$	8.553	8.781
Inferior Vena Cava	$E_{9,s}$	0.238	0.251

The remaining values show reasonable characteristics. For example, the resistances of the veins ($R_{i,s}$ for $i = 4, 7, 9$) and compliances of the veins ($E_{i,s}$ for $i = 4, 7, 9$) are smaller than their corresponding arteries and capillaries. This was expected as veins are more compliant vessels than arteries and capillaries as blood encounters little resistance when flowing from capillaries to veins. All resistances of the capillaries are also larger than their corresponding arteries. The systemic capillaries are made to be less compliant than their arteries, unlike the pulmonary artery and capillaries.

Table 4.3 shows the optimized initial volumes compared to the original starting volumes of each compartment. The overall volume of blood increased by almost 2 mL, within the reasonable range of volume for a newborn.

Table 4.3: Optimized RV-PA conduit initial volumes

Description	Volumes	Original	Optimized
Left Atrium	$V_1(RR)$	8.625	8.675
Right Atrium	$V_2(RR)$	3.450	3.470
Right Ventricle	$V_3(RR)$	12.938	13.012
Aorta	$V_4(RR)$	9.200	9.253
Pulmonary Artery	$V_5(RR)$	11.500	11.566
Pulmonary Capillaries	$V_6(RR)$	28.750	28.915
Pulmonary Vein	$V_7(RR)$	34.500	34.698
RV-PA Conduit	$V_8(RR)$	17.250	17.349
Upper Systemic Capillaries	$V_9(RR)$	9.200	9.253
Superior Vena Cava	$V_{10}(RR)$	86.250	86.745
Lower Systemic Capillaries	$V_{11}(RR)$	9.200	9.253
Inferior Vena Cava	$V_{12}(RR)$	86.250	86.745
Total Cardiovascular Volume		317.113	318.932

Figure 4.5 shows an additional investigation into the back-flow of blood from the right atrium into the left atrium. As shown in equations (2.24), (2.27), and (2.30), the pressure of each heart chamber has both an active and passive component. The reason for the back-flow is the sharp drop in pressure during the left atrium's contraction time (top right figure). This pressure is lower than the pressure of the right atrium, causing a pressure head moving from the right atrium into the left atrium while blood is flowing into the right ventricle as well.

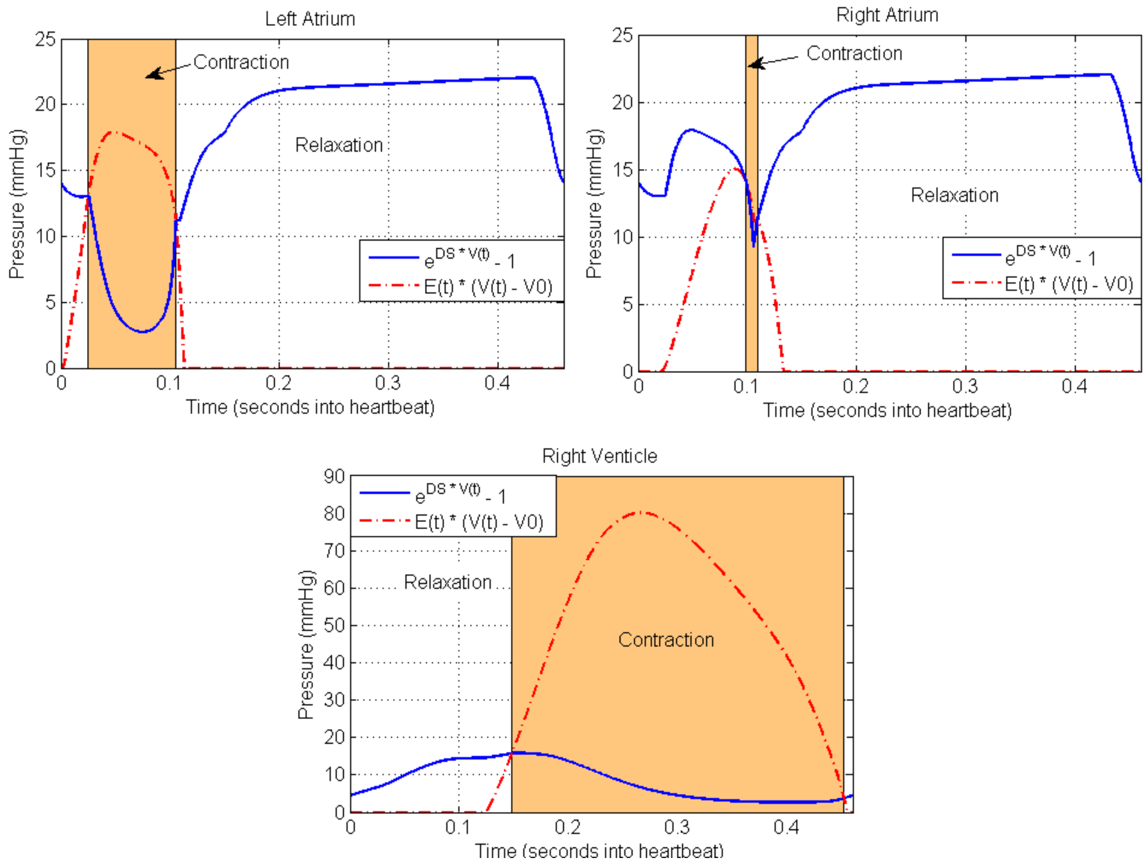

Figure 4.5: Passive vs. active pressure functions of the heart (RV-PA Conduit Model). In all three plots, the red dashed line is the modeled active pressure of the heart chamber and the blue solid line the passive. The top left plot shows the pressure modeling of the left atrium, the top right is the pressure modeling of the right atrium, and the bottom plot is the pressure modeling of the right ventricle.

4.2 BT Shunt Resulting Parameters

Figure 4.6 shows the resulting BT shunt P-V loop derived by `lsqnonlin` compared to the goal P-V loop. Once again, the optimizer reached its maximum number of evaluations of the objective function. Due to the diminishing returns observed in the behavior of the optimizer towards the end of the run, the parameter values were taken as nearly optimized. The stroke volume of this P-V loop, 16.9 mL, is within reasonable tolerance and the pressures fall into the range of 4.1 mmHg to 77.5 mmHg. While there are differences from the RV-PA conduit results (Figure 4.1), the decreased IVCT and IVRT are still present. Again, the bottom left corner's unanticipated behavior is explained by the atrial pressure creating the back-flow of blood from right atrium into the left. This effect is further illustrated in Figure 4.7. Also, the decreased IVCT is the result of the low systemic blood pressure causing the aortic valve to open earlier. A decreased IVCT is not an expected characteristic of the BT shunt, as the shunt is connected to the aorta directly, not the right ventricle.

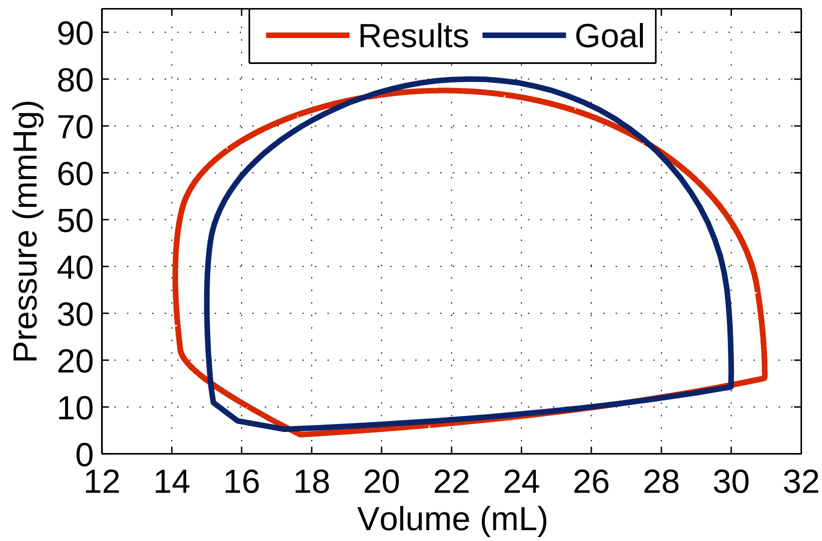

Figure 4.6: Resulting P-V loop of the BT shunt model. The goal P-V loop is shown in blue, and the resulting P-V loop from the optimizer in red.

Figures 4.7 to 4.9 show the volumes (top figure), pressures (middle figure), and flow (bottom figure) versus time for the heart, systemic system, and pulmonary system, respectively.

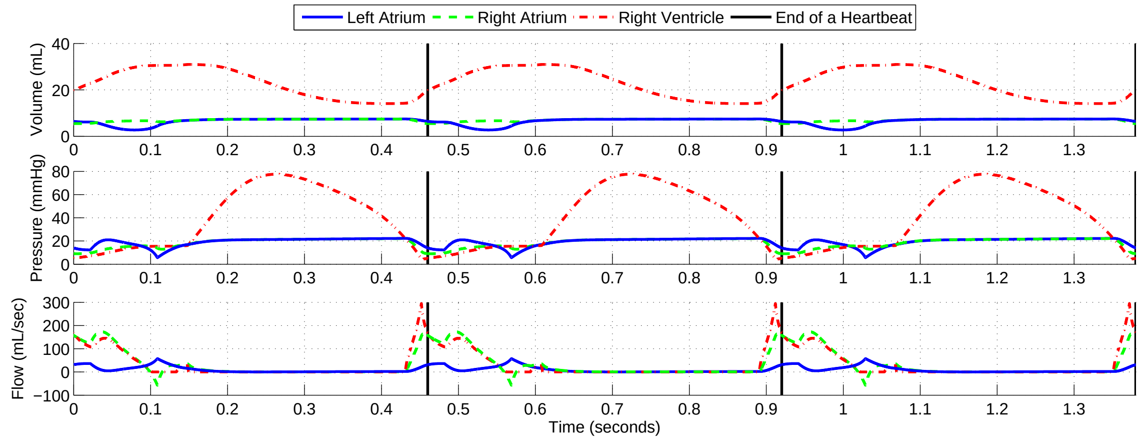

Figure 4.7: Volume, pressure, and flow of the heart vs. time of the BT shunt model. In all three figures the left atrium is shown in blue solid line, the right atrium in green dashed line, and right ventricle in the red dashed-dot line. Each heartbeat is delineated by a solid black line. The top plot is the volume vs. time, middle plot is pressure vs. time, and the bottom plot is the flow vs. time.

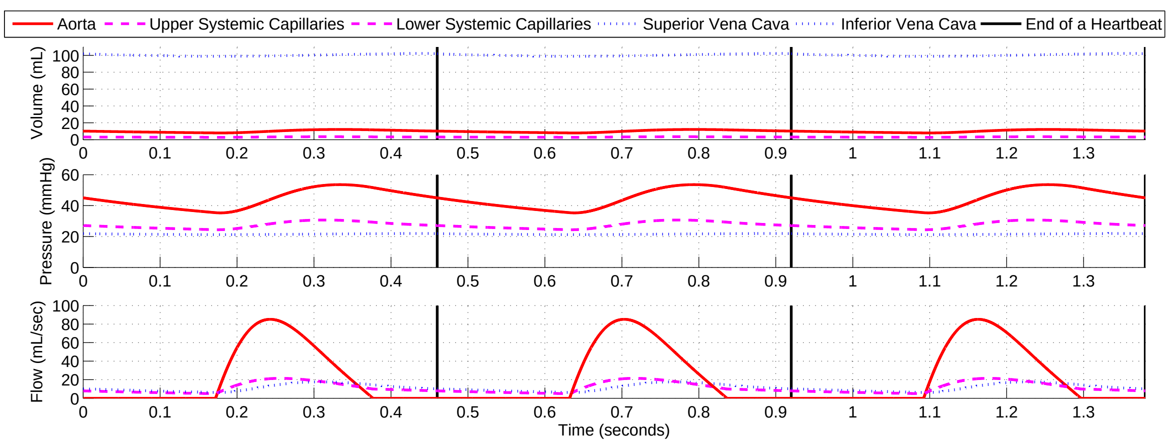

Figure 4.8: Volume, pressure, and flow of the systemic system vs. time of the BT shunt model. In all three figures the aorta is shown in the red solid line, the upper and lower systemic capillaries in the pink dashed line, and superior and inferior vena cavas in the blue dotted line. Each heartbeat is delineated by a solid black line. The top plot is the volume vs. time, middle plot is pressure vs. time, and the bottom plot is the flow vs. time.

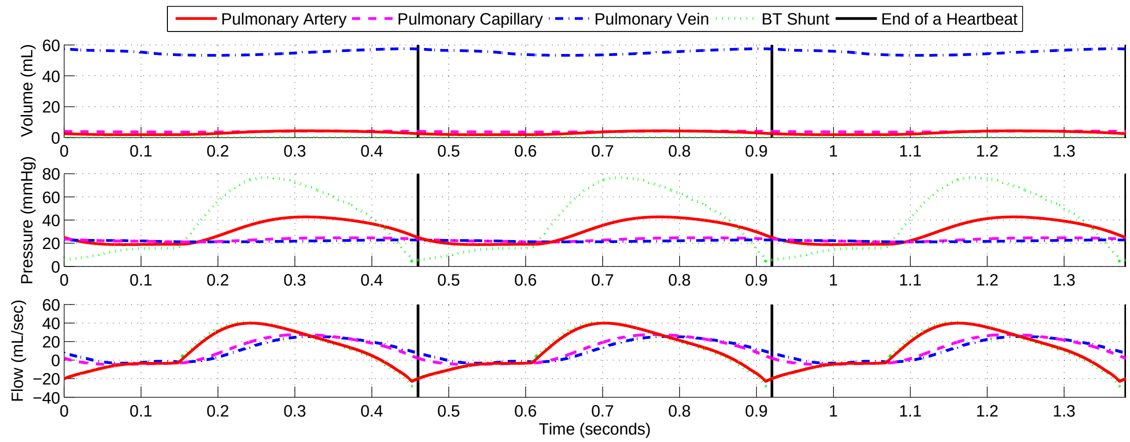

Figure 4.9: Volume, pressure, and flow of the pulmonary system vs. time of the BT shunt model. In all three figures the pulmonary artery is shown in the red solid line, the pulmonary capillary in the pink dashed line, pulmonary vein in the blue dashed-dotted line, and the RV-PA conduit in the green dotted line. Each heartbeat is delineated by a solid black line. The top plot is the volume vs. time, middle plot is pressure vs. time, and the bottom plot is the flow vs. time.

Tables 4.4 and 4.5 show the optimized parameters compared to the original parameters. These parameters are consistent in behavior with the resulting RV-PA conduit parameters.

Table 4.4: Optimized BT shunt heart parameters

Description	Parameter	Original	Optimized
Resistances			
Left Atrium	$R_{1,h}$	0.198	0.282
Right Atrium (from Left Atrium)	$R_{2,h}$	0.018	0.074
Right Atrium (from Lower Systemic)	R_{IVC}	0.198	0.282
Right Atrium (from Upper Systemic)	R_{SVC}	0.198	0.282
Right Ventricle	$R_{3,h}$	0.047	0.024
E_{max}			
Left Atrium	$E_{max,1,h}$	4.026	4.801
Right Atrium	$E_{max,2,h}$	1.884	1.718
Right Ventricle	$E_{max,3,h}$	3.773	3.774
Diastolic Stiffness			
Left Atrium	$DS_{1,h}$	0.432	0.422
Right Atrium	$DS_{2,h}$	0.432	0.422
Right Ventricle	$DS_{3,h}$	0.092	0.092

Table 4.5: Optimized BT shunt blood vessel parameters

Description	Parameters	Original	Optimized
Resistances			
Aorta	$R_{1,s}$	0.495	0.373
Pulmonary Artery	$R_{2,s}$	1.172	0.973
Pulmonary Capillaries	$R_{3,s}$	0.968	0.663
Pulmonary Vein	$R_{4,s}$	0.415	0.101
BT Shunt	$R_{5,s}$	0.003	0.023
Upper Systemic Capillaries	$R_{6,s}$	2.493	2.249
Superior Vena Cava	$R_{7,s}$	0.354	0.515
Lower Systemic Capillaries	$R_{8,s}$	2.493	2.249
Inferior Vena Cava	$R_{9,s}$	0.354	0.515
Inverse compliance			
Aorta	$E_{1,s}$	3.174	4.421
Pulmonary Artery	$E_{2,s}$	6.512	9.709
Pulmonary Capillaries	$E_{3,s}$	3.220	5.843
Pulmonary Vein	$E_{4,s}$	0.274	0.398
BT Shunt	$E_{5,s}$	278.394	236.334
Upper Systemic Capillaries	$E_{6,s}$	8.553	8.744
Superior Vena Cava	$E_{7,s}$	0.238	0.215
Lower Systemic Capillaries	$E_{8,s}$	8.553	8.744
Inferior Vena Cava	$E_{9,s}$	0.238	0.215

Table 4.3 shows the resulting initial volumes of the BT shunt model from the optimizer. As before, the volumes are just scaled equally from the original parameters, as the simulation runs enough iterations to converge on the proper volume of each vessel.

Table 4.6: Optimized BT shunt conduit initial volumes

Description	Volumes	Original	Optimized
Left Atrium	$V_1(RR)$	8.625	8.587
Right Atrium	$V_2(RR)$	3.450	3.435
Right Ventricle	$V_3(RR)$	12.938	12.881
Aorta	$V_4(RR)$	9.200	9.159
Pulmonary Artery	$V_5(RR)$	11.500	11.449
Pulmonary Capillaries	$V_6(RR)$	28.750	28.623
Pulmonary Vein	$V_7(RR)$	34.500	34.348
BT Shunt	$V_8(RR)$	17.250	17.174
Upper Systemic Capillaries	$V_9(RR)$	9.200	9.159
Superior Vena Cava	$V_{10}(RR)$	86.250	85.870
Lower Systemic Capillaries	$V_{11}(RR)$	9.200	9.159
Inferior Vena Cava	$V_{12}(RR)$	86.250	85.870
Total Cardiovascular Volume		317.113	315.716

Figure 4.10 shows the additional investigation into the modeling of the active and passive pressures of the heart chambers. We found the same results as in the RV-PA conduit model (Figure 4.5). However, the active pressure of the right atrium (top right figure of Figure 4.10) is never used in the the final BT shunt P-V loop. This fact further suggests that the modeling of the atrial pressure taking into account the atrial contraction is suspect, producing physiological inaccuracies (back-flow from the right atrium into the left atrium).

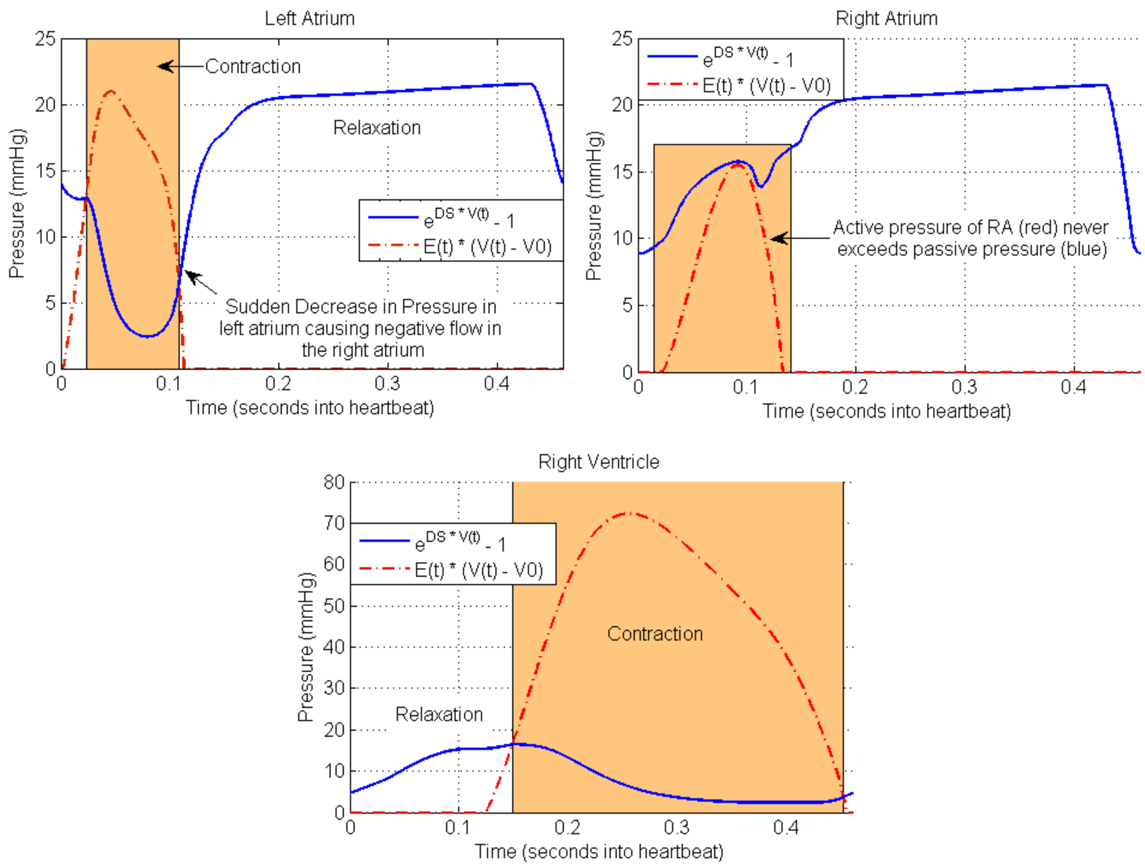

Figure 4.10: Passive vs. active pressure functions of the heart (BT Shunt Model). In all three plots, the red dashed line is the modeled active pressure of the heart chamber and the blue solid line the passive. The top left plot shows the pressure modeling of the left atrium, the top right is the pressure modeling of the right atrium, and the bottom plot is the pressure modeling of the right ventricle.

Chapter 5
CONCLUSION

We were able to improve the HLHS cardiovascular model presented in [Kad12] and move towards producing a right ventricular P-V loop that displays desirable characteristics for both commonly used surgical variants of the Norwood procedure. A correction included in our model is the conservation of blood volume, achieved by removing the coronary artery blood vessel whose contribution to the model was negligible. Another key difference between the two models is the numerical method used to solve the system of ODEs. Applying the advanced general-purpose solver `ode15s` to the system reduced the run-time of the model from over a minute for 100 cycles to 20 seconds. Our model also provides future researchers without extensive MATLAB knowledge the ability to explore the effects of the model parameters through a GUI and see the resulting right ventricular P-V loop and volumes, pressures, and flows versus time for some of the modeled compartments.

To identify parameters that produced a ventricular P-V loop that best fit desired characteristics such as stroke volume and maximum and minimum pressures, a nonlinear least-squares optimization was performed using the MATLAB function `lsqnonlin`. For the RV-PA conduit model, the optimized P-V loop had a stroke volume of 16.6 mL and pressures in the interval $[3.8, 80.1]$. While this P-V loop showed the expected decrease in IVCT as compared to a healthy heart, the IVRT did not have the expected results. The optimized BT shunt ventricular P-V loop showed comparable results; its optimized P-V loop had a stroke volume of 16.9 and pressures within the interval $[4.1, 77.5]$.

While the decreased IVCT time is expected for the RV-PA conduit model, it was not for the BT shunt model. Further investigation revealed that the systemic blood pressure was much lower than the pulmonary blood pressure in both models. This lower blood pressure potentially could be causing the aortic valve to open early (equation (2.34)-(2.35)), thus causing the reduced IVCT. Also, since the pulmonary cardiovascular system and systemic cardiovascular system both branch from the aorta in the BT shunt model, the lower pulmonary blood pressure was creating a vacuum and pulling blood from the body into the pulmonary system. Future work should be done to try to increase the systemic blood pressure and to determine if the decreased IVCT is still present in both models to a lesser extent in the RV-PA conduit model, or removed completely from the BT shunt model.

Further investigation into the pressure vs. time plots for the atria revealed an unanticipated back-flow of blood from the right atrium and into the left atrium. This was a result of the atrial modeling of contractility. Further work should be done exploring other models for the atrial contractility and pressure. In addition to the modeling of contractility of the atria, the contractility of the right ventricle should be explored to evaluate other models of the pressure of the various heart chambers and their effects on the results. The unexpected IVRT behavior can be attributed to the modeling of the contractility of the ventricle, which is affecting the formula for computing pressure during contraction. Another possible reason for the observed back-flow could be one of the assumptions about blood being an incompressible Newtownian fluid with no inertance. This assumption is allowing for the instantaneous change in direction of the flow without accounting for the momentum of the fluid.

Additional future modifications to the current model for both the RV-PA conduit and BT shunt may include modeling the O_2 saturation, the reincorporation of the coronary artery into the model, and validation of the optimized ventricular P-V loops with actual patient data. The model could also be revisited to remove components of the model to further simplify the current model.

BIBLIOGRAPHY

[ALSE72] S. Sultan Ahmed, Gilbert E. Levinson, Carl J. Schwartz, and Philip O. Ettinger, *Systolic time intervals as measures of the contractile state of the left ventricular myocardium in man*, Circulation **46** (1972), 559–571.

[AMSA13] Saif Anwaruddin, Joseph M. Martin, John C. Stephens, and Arman T. Askari (eds.), *Cardiovascular hemodynamics an introductory guide*, Contemporary Cardiology, Springer, 2013.

[APH05] Robert H. Anderson, Marco Pozzi, and Suzie Hutchinson, *Hypoplastic left heart syndrome*, Springer-Verlag, 2005.

[BKD+09] David J Barron, Mark D. Kilby, Ben Davies, John G. C. Wright, Timothy J. Jones, and William J Brawn, *Hypoplastic left heart syndrome*, Lancet **374** (2009), 551–564.

[BMdL+08] Edward L. Bove, Francesco Migliavacca, Marc R. de Leval, Rossella Balossino, Giancarlo Pennati, Thomas R. Lloyd, Sachin Khambadkone, Tain-Yen Hsia, and Gabriele Dubini, *Use of mathematic modeling to compare and predict hemodynamic effects of the modified blalocktaussig and right ventriclepulmonary artery shunts for hypoplastic left heart syndrome*, The Journal of Thoracic and Cardiovascular Surgery **136** (2008), no. 2, 312–320.

[BS93] Ofer Barnea and Nadav Sheffer, *A computer model for analysis of fluid resuscitation*, Computers in Biology and Medicine **23** (1993), no. 6, 443–454.

[Dis11] *Facts about hypoplastic left heart syndrome*, Website: http://www.cdc.gov/ncbddd/heartdefects/hlhs.html, September 2011.

[EMS+07] Linda Edwards, Kevin P. Morris, Ameen Siddiqui, Deborah Harrington, David Barron, and William Brawn, *Norwood procedure for hypoplastic left heart syndrome: BT shunt or RV-PA conduit?*, Archives of Disease in Childhood: Fetal & Neonatal **92** (2007), no. 3, 210–214.

[FLTV06] Luca Formaggia, Daniele Lamponi, Massimiliano Tuveri, and Alessandro Veneziani, *Computer methods in biomechanics and miomedical engineering*, Computer Methods in Biomechanics and Biomedical Engineering **9** (2006), no. 5, 273–288.

[FV03] L. Formaggia and A. Veneziani, *Reduced and multiscale models for the human cardiovascular system*, Tech. Report I-20133, MOX, Mathematics Department, Milan, Italy, May 2003.

[HCC+11] Tain-Yen Hsia, Daria Cosentino, Chiara Corsini, Giancarlo Pennati, Gabriele Dubini, and Francesco Migliavacca, *Use of mathematical modeling to compare and predict hemodynamic effects between hybrid and surgical norwood palliations for hypoplastic left heart syndrome*, Circulation **124** (2011), S204–S210.

[Iai09] Paul A. Iaizzo (ed.), *Handbook of cardiac anatomy, physiology, and devices*, Springer, 2009.

[Kad12] Evgeny Kadner, *Comparison between the effects of Blalock-Taussig shunt and Sano shunt on the hemodynamic profile after stage I Norwood palliation, immediate following the operation and during first 6 months of growth - a model study*, Master's thesis, TEL AVIV UNIVERSITY, January 2012.

[Khu06] Indu Khurana, *Textbook of medical physiology*, Elsevier, 2006.

[Kla11] Richard E. Klabunde, *Cardiovascular physiology concepts*, Website: http://www.cvphysiology.com/Cardiac%20Function/CF024.htm, May 2011.

[LB92] Matthew N. Levy and Robert M. Berne, *Cardiovascular physiology*, 6 ed., vol. Cardiovascular Physiology, Mosby-Year Book, Inc, January 1992.

[Mil90] William R. Milnor, *Cardiovascular physiology*, Oxford UniversiSpringer, Inc, 1990.

[MMW+11] Tomasz Mroczek, Zbigniew Malota, Elzbieta Wojcik, Zbigniew Nawrat, and Janusz Skalski, *Norwood with right ventricle-to-pulmonary artery conduit is more effective than norwood with blalocktaussig shunt for hypoplastic left heart syndrome: mathematic modeling of hemodynamics*, European Journal of Cardio-thoracic Surgery **40** (2011), 1412–1418.

[OSM+10] Richard G. Ohye, Lynn A. Sleeper, Lynn Mahony, Jane W. Newburger, Gail D. Pearson, Minmin Lu, Caren S. Goldberg, Sarah Tabbutt, Peter C. Frommelt, Nancy S. Ghanayem, Peter C. Laussen, John F. Rhodes, Alan B. Lewis, Seema Mital, Chitra Ravishankar, Ismee A. Williams, Carolyn Dunbar-Masterson, Andrew M. Atz, Steven Colan, L. LuAnn Minich, Christian Pizarro, Kirk R. Kanter, James Jaggers, Jeffrey P. Jacobs, Catherine Dent Krawczeski, Nancy Pike, Brian W. McCrindle, Lisa Virzi, and J. William Gaynor, *Comparison of shunt types in the Norwood procedure for single-ventricle lesions*, The New England Journal of Medicine **362** (2010), no. 21, 1980–1992.

[San12] William P. Santamore, *Private communication*, 2012.

[SLH11] Yubing Shi, Patricia Lawford, and Rodney Hose, *Review of zero-d and 1-d mmodel of blood flow in the cardiovascular system*, BiomMedical Engineering OnLine **10** (2011), 33.

[SS74] Hiroyuki Suga and Kiichi Sagawa, *Instantaneous pressure-volume relationships and their ratio in the excised, supported canine left ventricle*, Circulation Research **34** (1974), 117–126.

[SSB07] Liron Sheffer, William P. Santamore, and Ofer Barnea, *Cardiovascular simulation toolbox*, Cardiovascular Engineering **7** (2007), 81–88.

[TMR+01] Wayne Tworetzky, Doff B. McElhinney, V. Mohan Reddy, Michael M. Brook, Frank L. Hanley, and Norman H. Silverman, *Improved surgical outcome after fetal diagnosis of hypoplastic left heart syndrome*, Circulation **103** (2001), 1269–1273.